A Quantitative Model for Decompression Surgery in Bell's Palsy

by

Ronit Malka

Submitted in Partial Fulfillment of the Requirements for the M.D. Degree with Honors in a Special Field at Harvard Medical School

May 1, 2019

Area of Concentration:	**Otolaryngology**
Project Advisor:	**Dr. Tessa Hadlock**
Author's Prior Degrees:	**B.S.**

I have reviewed this thesis. It represents work done by the author under my supervision and guidance.

Table of Contents

Table of Figures

ABSTRACT

Bell's palsy is an idiopathic mononeuritis of the facial nerve thought to result from viral reactivation, causing inflammation and subsequent compression of the nerve within the rigid confines of the temporal bone. While most affected patients eventually recover normal facial function, aberrant neural regeneration occurs in a subset of Bell's patients who present with severe facial weakness at onset, resulting in permanent facial synkinesis and disfigurement. Neural decompression surgery to alleviate pressure on the facial nerve in the acute setting of severe Bell's palsy has been advocated as means to reduce risk of development of long-term sequelae, but use of this procedure has been limited and its efficacy is not well understood. Described is the design and validation of a rat model for unilateral compressive neuropathy of the facial nerve with the ability to examine long-term functional recovery associated with various durations and degrees of neural compression. Animals were implanted with vascular occlusion cuffs around branches of the facial nerve controlling whisker movements on one side, and cuffs inflated to various pre-set pressures for five to seven days. Whisking activity was quantified daily to characterize the threshold extrinsic pressure required to induce palsy. Cuffs were then be deflated and explanted, and whisking activity tracked and compared between sides over the ensuing 10 weeks. Functional nerve recovery and histological analysis of compressed nerves were then evaluated to determine the pressure range in which a Bell's-like phenomenon is observed in this rat model. This work is the first to characterize the relationship between neural compression pressure and long-term recovery of facial function in highly quantitative and controlled fashion in a live animal model. Future work will seek to characterize the relationship between the timing of neural decompression and long-term facial function, providing evidence to support or refute the utility of mechanical decompression of the facial nerve in the setting of acute Bell's palsy.

ACKNOWLEDGEMENTS

I would like to thank my thesis advisors and principal investigators Dr. Tessa Hadlock and Dr. Nate Jowett for their incredible and enthusiastic mentorship, both in academic research and in clinical medicine, and for their endless help and support as I completed this project. I am incredibly grateful for the help of Pavel Gorelik and Dr. Ofer Mazor at the Harvard Instrumentation Facility for their bottomless advice on electrical engineering design and manufacture, as well as an occasional baklava, and to Dr. Matthew Frosch for leading me to finding the Instrumentation Facility. A sincere thank you as well to our lab manager Christopher Knox and postdoctoral fellows Dr. Jacqueline Green, Dr. Suresh Mohan, Dr. Diego Guarin and Dr. Iván Coto Hernández for their teaching, support, and guidance throughout the project. Finally, thank you to Dr. Robert Wood and the Harvard Microrobotics Laboratory for allowing me to use lab equipment for device fabrication. This project was conducted with funding from the Surgical Photonics & Engineering Laboratory at Massachusetts Eye and Ear Infirmary and the Air Force Institute of Technology.

GLOSSARY OF ABBREVIATIONS

AAO-HNSF	American Academy of Otolaryngology – Head and Neck Surgery Foundation
ADC	Analog-to-digital converter
BP	Bell's palsy
CMAP	Compound muscle action potential
CN	Cranial nerve
EMG	Electromyography
ENoG	Electroneurography
ESN	Electronic serial number
FNGS	Facial Nerve Grading Scale
HBGS	House-Brackmann grading scale
HSV	Herpes simplex virus
MCF	Middle cranial fossa
MUAP	Motor unit action potential
PCB	Printed circuit board
PNI	Peripheral nerve injury
SMAS	Superficial musculoaponeurotic system
VZV	Varicella zoster virus

1 INTRODUCTION

Bell's palsy (BP) is a disease of idiopathic onset that results in facial palsy, typically of unilateral distribution, on either side of the face [1, 2]. Palsy progresses rapidly over the course of 1-3 days, and can lead to partial or total loss of facial mimetic function on the affected side of the face. BP accounts for the majority of facial palsies worldwide, with an incidence of about 30 per 100,000; 85% of cases resolve spontaneously, with little to no residual symptoms [3, 4]. However, the remaining 10-15% of patients progress to develop facial contractures, fasciculations, and synkinesis, believed to be the result of aberrant reinnervation (axonal extension to inappropriate muscles); these patients experience a significant decline in their quality of life due to aesthetic, communicative, and functional impairments. While the most widely accepted mechanism behind BP is viral reactivation in the facial nerve, the exact pathophysiology of BP remains unknown and is contested among physicians of different specialties [5]. There is also debate over how to treat patients presenting with BP in both the acute and chronic setting, varying from minimal medical therapy to electromyography and surgical decompression [5-7]. This introduction will give a brief background on the mechanisms behind and current methods of assessing neural injury before addressing the pathophysiology behind BP, why poor outcomes occur, how these poor outcomes are treated, and why a quantitative, unbiased animal model is needed to better understand these outcomes.

1.1 PATHOPHYSIOLOGY OF NERVE INJURY

1.1.1 WALLERIAN DEGENERATION

Coined by Augustus Waller in 1850, Wallerian degeneration refers to the degeneration of axons distal to a site of injury, classically a transection injury [8, 9]. Studies with the slow Wallerian degeneration (Wld^s) mutant mouse has demonstrated that other, more common forms of neural injury such as compression, tension, toxic insult, or and some inherited neuronal disorders also show degeneration in a similar pattern and using similar mechanisms, coined Wallerian-like degeneration [8]. After initial injury, the distal

portions of transected axons remain anatomically intact and capable of propagating extrinsically evoked action potentials for up to 3-5 days[1] [9].

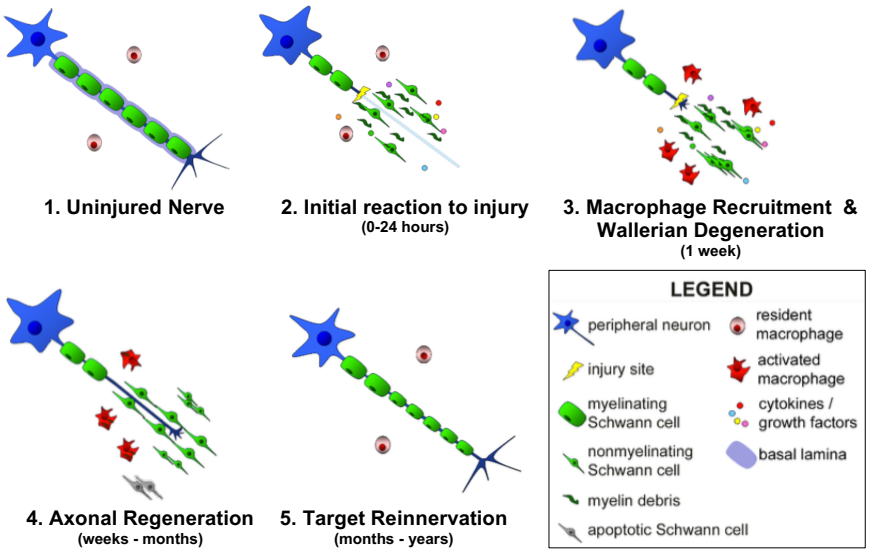

Figure 1: Wallerian degeneration progression over time, demonstrating early immune response and anterograde Schwann cell loss followed by subsequent remyelination along existing perineureum or epineurium. Adapted from Gaudet et al. [9]

As diagrammed in Figure 1, the initiating event in degeneration is the granular disintegration of the cytoskeleton, which is instigated by calcium influx to the axon after a 3-4 day delay and rapidly proceeds over the course of about one hour. Once the axons are destroyed the surrounding Schwann cells begin directing further degenerative processes, recruiting inflammatory cells and phagocytosing debris themselves. Schwann cells also dedifferentiate at this stage, ceasing production of neurotoxic myelin in favor of proliferation. While recruited immune cells and Schwann cells clear cellular debris to make way for axonal regeneration, axons prepare for regeneration; triggered by trophic factors secreted by surrounding Schwann cells, neuronal cell bodies hypertrophy and begin preparation for growth cone formation. After a lag period of weeks to months, the growth cone is fully formed and can travel along intact endoneurial tubes, tubes of thin connective tissue remaining from the original nerve sheath or laid down by proliferating Schwann cells. Axonal outgrowth is promoted by continued Schwann cell trophic factor

[1] Wallerian degeneration proceeds about twice as quickly in rodents as in humans, showing degeneration in 24-48 hours as opposed to 3-4 days [9].

[2] While precise calculation of the density of a glycerol:water mixture is subject to a contraction coefficient,

release and, if able to proceed along the entire course of the distal stump, can reconnect with the distal target and complete reinnervation. However, if endoneurial integrity is compromised due to severe damage, poor Schwann cell support of regeneration, or slow axonal outgrowth, the nerve may either fail to regenerate or begin to regenerate aberrantly and innervate inappropriate peripheral targets, a clinical sign known as synkinesis.

1.1.2 CLASSIFICATION OF PERIPHERAL NERVE INJURY

The first widely accepted form of classifying peripheral nerve injury (PNI) came in 1943 with Seddon's definitions of neurapraxia, axonotmesis, and neurotmesis [10]. Neurapraxia is the mildest form of injury, representing a conduction block and local myelin injury without any loss of continuity in the axons, epineurium, perineurium, or endoneurium. Intact AP conduction is seen if stimulated distal to the site of conduction block, and no Wallerian degeneration proceeds. Once the conduction block is relieved, the nerve will fully recover. Axonotmesis describes a loss of continuity of the axon bundle and local myelin damage, with intact connective tissue of the endoneurium, perineurium and epineurium; Wallerian degeneration occurs, resulting in loss of evoked AP conduction after 3-4 days. The nerve can spontaneously regenerate over the course of months via axonal outgrowth following Wallerian degeneration, but recovery may be complicated by poor Schwann cell or inflammatory response, poor growth cone formation, or scar formation. Neurotmesis describes complete nerve transection, resulting in Wallerian degeneration; however, because the endoneurial sheath is transected, the nerve will not regenerate without surgical repair. These terms are still widely used today to describe PNI.

While the Seddon classification has proven very useful in understanding PNI, the need for a more precise mechanism of characterizing PNI, especially severe forms, became apparent [11]. In 1951 the Sunderland classification system was published, which grades PNI on a scale from class I to class V. Class I injury is synonymous with Seddon's definition of neurapraxia and class II injury is synonymous with Seddon's definition of axonotmesis. Classes III-V further define gradations of neurotmesis based on the three main layers of a nerve (endoneurium, perineurium, and epineurium); class III injury has damaged endoneurium, class IV has damaged endoneurium and

perineurium, and class V has full transection of the entire nerve with damage to the endoneurium, perineurium, and epineurium.

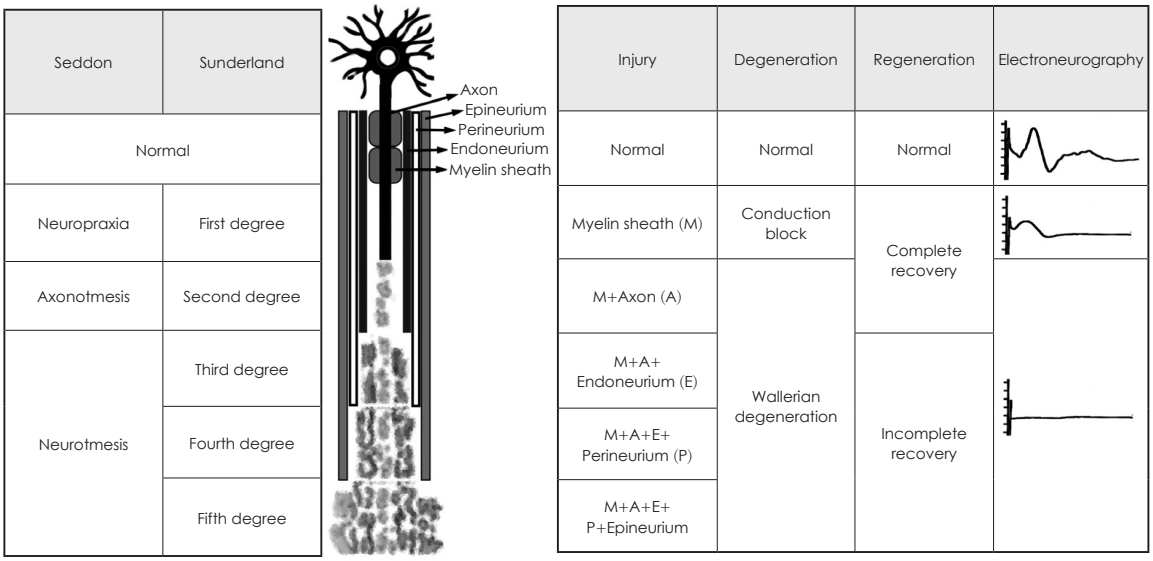

Figure 2: Comparison of the Seddon and Sunderland classifications of neuronal injury with degenerative, regenerative, and electrodiagnostic outcomes. Image taken from Lee [12].

1.1.3 COMPRESSION NEUROPATHY

Entrapment neuropathies, also known as compression neuropathies, are vexing clinical conditions that affect more than 40 million people worldwide every year and can result in chronic pain, numbness, muscle weakness, and spasticity [13, 14]. Entrapment neuropathies have been documented in almost all major peripheral nerves, including cranial nerves, spinal nerve roots, nerves of the trunk, and upper and lower extremities [15]. The underlying mechanism is thought to be mechanical pressure, either externally applied or from nerve edema within an enclosed space [16]. Acutely this can lead to focal demyelination, which can be completely reversible if the mechanical insult is removed before axonal degeneration can progress. However, in severe or chronic cases, axonal transport of nutrients can become disrupted, leading to Wallerian-like axonal degeneration and permanent loss of nerve conduction [9]. A variety of motor and sensory nerves may become entrapped resulting in clinical sequelae. Of these, the median nerve is most susceptible to entrapment, resulting in carpal tunnel syndrome. Owing to differences in entrapment severity, location, nerve size, and chronicity, the clinical course of various entrapment neuropathies may differ considerably [15, 17]. Treatment of entrapment neuropathies is similarly varied – while decompression surgery

is a common treatment, the prevalence and efficacy of these procedures vary widely based on location of the neuropathy. Thus, while 30% or more of carpal tunnel cases are surgically decompressed every year, fewer than 5% of cranial nerve entrapment neuropathies are treated by decompression surgery annually [5, 14].

1.1.4 NOMENCLATURE

The terms paresis, palsy, and paralysis are often used somewhat interchangeably in the literature and have caused confusion in retrospectively assessing data related to BP course and recovery [18]. Because the expected outcomes in BP are highly dependent upon degree of functional loss, being deliberate with the use of these words is vital to accurately describing all work related to BP [17, 18]. The term “paresis” is usually used to refer to muscle weakness without total loss of function and “paralysis” to refer to 100% loss of muscle function; the term “palsy” refers to general loss of function that can encompass paresis or paralysis, with the classification of “complete palsy” being synonymous with paralysis and “incomplete palsy” being synonymous with paresis [18].

1.2 BELL’S PALSY: AN OVERVIEW

1.2.1 DEFINITION AND PRESENTATION

According to the AAO-HNSF, BP is defined as “acute unilateral facial nerve paresis or paralysis with onset in less than 72 hours and without an identifiable cause”[7]. While the diagnosis of BP is often inappropriately applied to other idiopathic facial paralyses with acute but non-instantaneous onset (as opposed to stroke or transient ischemic attack), BP is primarily a diagnosis of exclusion and is not an applicable diagnosis to paralysis from trauma, malignancy, or direct infection [1, 7].

The symptoms of BP arise from dysfunction of the CN VII, whose primary function is branchial motor innervation of the muscles of facial expression. Approximately 15-30% of patients diagnosed with BP experience incomplete flaccid paralysis, while the remaining 70-85% experience total paralysis [17].

Figure 3: Post-paralytic right facial palsy and synkinesis, demonstrated with (A) involuntary eye closure with pucker, (B) neck contraction with smile, and (C) impaired oral commissure excursion and involuntary eye closure with smile. Images used with permission from Facial Nerve Center, Massachusetts Eye and Ear Infirmary.

CN VII also provides motor innervation to the stapedius muscle, general sensory fibers to the outer ear, special sensory fibers for taste via the chorda tympani, and visceral motor fibers for salivary and tear secretion via the greater petrosal nerve; thus, BP often also presents with taste disturbances, dry mouth, dry eyes, and/ or hearing disturbances, specifically hyperacusis [1, 7, 13]. The frequent inclusion of symptoms relating to chorda tympani and greater petrosal dysfunction suggest the damage to the nerve extends very proximally, nearer the nerve's entrance to the fallopian canal of the temporal bone at the internal acoustic meatus.

1.2.2 PATHOPHYSIOLOGY

While the exact etiology of BP remains unclear, current consensus among researchers and physicians today is that BP arises from viral reactivation and its potential sequelae, which are most frequently cited as Schwann cell death, compression secondary to inflammation and edema, and ischemia secondary to compression [1, 7, 19]. BP is differentiated from other idiopathic facial paralyses like Ramsay Hunt syndrome by (a) being a mononeuritis, i.e. constituting a specific attack on the facial nerve (CN VII) without other cranial nerve involvement, and (b) the proposed mechanism of herpes simplex virus reactivation in the geniculate ganglion [20] [3, 4]. More recent work has implicated other viral agents, specifically varicella-zoster virus (VZV), influenza, and human herpes virus 6 (HHV-6) [21-24]).

It is postulated that upon reactivation, the causative virus rapidly infects Schwann cells along the facial nerve and results in inflammation, demyelination, and axonopathy [3]. Demyelination has been cited by some as the sole cause of neural dysfunction and eventual damage in BP [6]. However, there is also a hypothesis that the acute symptoms and much of the lasting axonal damage induced in BP stem not from demyelination but rather Wallerian degeneration due to secondary nerve compression within the temporal bone caused by the inflammatory response to viral reactivation [3, 25-27]. This mechanism is contested and is described in greater detail later in this introduction (see Section 1.3).

1.2.3 DEMOGRAPHICS AND RISK FACTORS

While BP can affect all age groups starting from infancy, most patients present between the ages of 15 and 45 [17]. More women present with BP than men, though it is unclear whether this could be an immune mechanism or is due to confounding from female-specific risk factors such as pregnancy and preeclampsia. Patients with diabetes, obesity, or hypertension are at increased risk for BP, as are patients with upper respiratory pathology [7].

1.2.4 FACIAL NERVE GRADING SYSTEMS

For assessing facial nerve damage in particular, a number of facial nerve grading systems have been developed [28, 29]. The most widely-used and influential of these systems is the House-Brackmann facial nerve grading system (HBGS), adopted by the American Academy of Otolaryngology – Head and Neck Surgery Foundation (AAO-HNSF) in 1984 [28]. The HBGS assigns a grade of I-VI based on two semi-quantitative measures (oral commissure and eyebrow displacement, each a scale of 1-4 by binning displacement in 0.25cm increments) and one qualitative measure of functionality, a composite assessment of specific muscle groups' function and presence or absence of contracture, synkinesis, or hemifacial spasm. While still cited frequently in assessing the degree of facial nerve dysfunction, the HBGS has been criticized for its subjective nature, ambiguity in handling secondary defects such as synkinesis, contracture, and spasm, and its very gross grading of facial nerve dysfunctional.

In an attempt to address the deficits in the HBGS, other grading systems have been developed. In 1986 the Burres-Fisch system was introduced, addressing the HBGS

subjectivity by relying solely on a complex set of facial measurements. However, this method took as long as 20 minutes to complete and did not provide a mechanism to account for secondary defects, both of which made it clinically difficult to implement. The Nottingham system, a modification to the Burres-Fisch system proposed in 1994, attempted to retain objectivity by incorporating fewer, simpler quantitative measures; while taking much less time to complete, it also was unable to account for secondary defects and was thus of little clinical utility. The 1996 Sunnybrook scale swung in the opposite direction, attempting to grade based on purely subjective measures of secondary defects. Since the early 2000s a number of computational grading systems have arisen, including pixel subtraction, landmark tracking, and 3D mapping. While these objective systems have been shown to be as good or better than the HBGS, they require additional software that many centers are unable or unwilling to buy or develop. The added benefit of such unbiased or quasi-unbiased grading scales has not to date been enough to garner wide acceptance in grading facial nerve dysfunction in a clinical setting.

In 2009 the HBGS, also referred to as the Facial Nerve Grading Scale (FNGS), was revised to reduce ambiguity in handling secondary defects [29]. Coined the FNGS 2.0, this system uses a combination of five subjective ratings, four kinetic (motion of the eyebrow, eye, nasolabial fold, and oral commissure) and one synkinetic. This is now accepted by the AAO-HNSF as the standard grading scale for assessing facial nerve dysfunction. However, many clinicians still feel this grading scale is still too limited and objective, and additional work into a broader, more standardized grading scales continues. Notable among these is the eFACE, a semi-automated clinical tool encompassing sixteen static and dynamic measures, including synkinesis[30, 31].

1.2.5 ELECTRODIAGNOSTICS

Evaluation of the degree of Wallerian degeneration a nerve has undergone can prognosticate outcome in patients with acute BP [32]. The current method of evaluating degree of nerve degeneration is a two-step electrodiagnostic process, summarized in Figure 4, derived from the combined works of Fisch in 1981 and Gantz et al in 1999 [13, 25, 26].

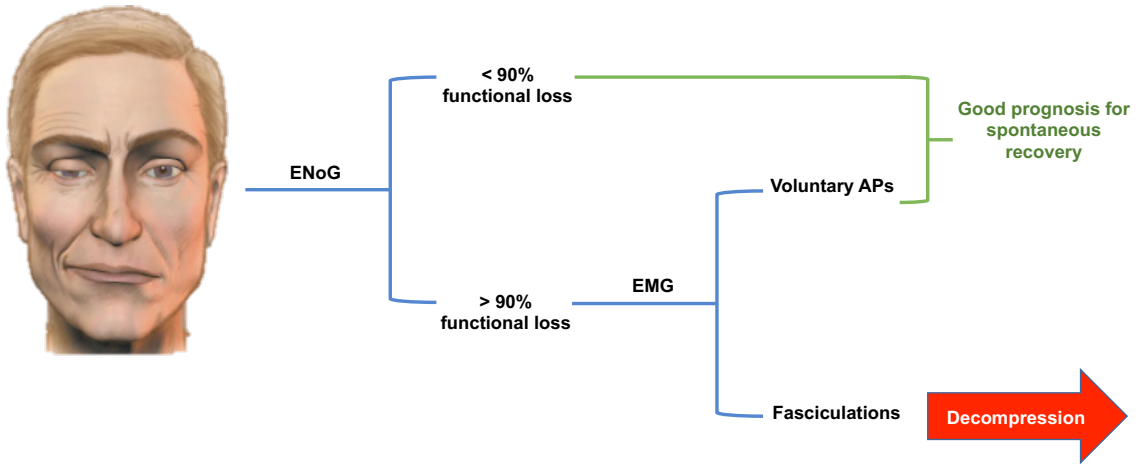

Figure 4: Diagram of two step electrodiagnostic pathway for Bell's Palsy using ENoG and EMG to decide whether decompression surgery is indicated for a patient. Image created with modification of figure from Gilden [13].

The first step in the electrodiagnostic pathway is electroneurography (ENoG), also known as evoked electromyography (EMG). ENoG consists of electrical stimulation distal to the site of injury to the facial nerve as it exits the stylomastoid foramen and measurement of the compound muscle action potential (CMAP) at its distal targets. The CMAP of the affected side is compared as a percentage to the CMAP of the unaffected side. ENoG showing less than 90% degeneration is predictive of good outcome, while ENoG showing greater than 95% degeneration predicts a poor outcome and was identified as inclusion criteria for decompression surgery in Fisch's study [25]. Using these criteria, ENoG has excellent negative predictive value (80-100%) and fair positive predictive value (50-90%)[32]. In this way, ENoG differentiates patients whose facial nerves have begun to undergo Wallerian degeneration (second-to-fifth degree injuries on the Sunderland scale, or axonotmesis/neuronotmesis on the Seddon scale) from first degree (i.e. neurapraxic only) insults. Because evoked stimulation of the facial nerve outside of an operating theatre is possible only for the extratemporal segment (i.e., distal to the site of neural conduction blockade at the meatal foramen within the temporal bone), clinical ENoG provides no useful data when performed earlier than 72 hours following palsy onset, as Wallerian degeneration occurs slowly over a three to five day period.

However, patients with first degree axonal injuries may have ENoG showing greater than 95% loss. This is likely due to the short timescale across which ENoG operates (100 ms recordings), which may be inadequate to detect action potential conduction across the

nerve due to asynchronous firing of incompletely blocked neurapraxic fascicles. This does not allow for accurate prognostication for patients outside of the acute phase of injury who may have undergone second degree injury but. In order to account for these patients, a second electrodiagnostic step of EMG can be performed, which evaluates for individual motor unit action potentials (MUAP) measured at a number of at the nerve's distal targets (usually orbicularis oclui and orbicularis oris, but may also include levator labii superioris, frontalis,and mentalis). If MUAPs are present, this suggests that sufficient neural continuity remains, and the degree of neural insult is likely not severe enough to result in long-term dysfunction. If, however, no MUAPs are present (i.e. EMG demonstrates only fasciculations indicative of motor unit denervation), the predicted outcome is poor and decompression surgery is indicated. Based on Fisch's initial criteria of performing decompression surgery within 14 days of symptom onset, and EMG may be performed up to 14 days after symptom onset to determine the state of the facial nerve endoneurium and thus the predicted outcome for that patient as close to time for decompression as possible. Additionally, EMG may be tracked through 14 days for a particular patient to evaluate for degeneration of MUAPs and thus changing clinical course and evolving indications for surgical intervention.

1.2.6 OUTCOMES

Without treatment, approximately 85% of BP patients will spontaneously recover full function within several weeks of onset, while the remaining 15% might not see any signs of recovery for 3- 4 months, with full evolution of recovery lasting up to 12-18 months [17]. There is markedly improved odds of full recovery of normal facial function in patients exhibiting incomplete palsy; 94% of patients presenting with incomplete palsy ultimately regain normal function spontaneously, while only 70% of patients presenting with complete palsy fully recover [7, 17]. A positive correlation between functional recovery and recovery rate is also seen: an 88% recovery rate has been observed in patients exhibiting recovery within a week, dropping to 83% in two weeks and 61% in three weeks [17]. For those patients who do not achieve full functional recovery, undesirable outcomes such as synkinesis, contracture, and retained paresis or palsy can be seen.

1.2.7 TREATMENT

To date, the only treatment of BP showing clinically significant improvements in outcome in adequately powered studies is steroid therapy [1, 33]. Treatment with anti-virals has shown mixed results, with some studies suggesting benefit while others show no effect [1, 33, 34]. Surgical decompression has also had variable acceptance in literature, with some studies showing no difference in outcome compared to steroid treatment while others show markedly improved functional recovery [19, 33]; the data behind surgical decompression is analyzed in greater depth later in this introduction (see section "Surgical Decompression"). Other treatment modalities such as physical therapy and acupuncture have been evaluated to a lesser degree show little effect [35]. In 2013, the AAO-HNSF published an updated clinical practice guideline delineating current standards in the diagnosis and treatment of BP [7]. Therein, it is recommended that all patients 16 years or older be put on oral steroids within 72 hours of symptom onset. Antirvirals given in conjunction with steroids are optional, as is electrodiagnostics for patients exhibiting complete palsy. Antiviral monotherapy and electrodiagnostics for patients exhibiting incomplete palsy is strongly discouraged. Decompression surgery, as alongside acupuncture and physical therapy, are mentioned as options without recommendation for or against based on poor quality of data surrounding these treatments. While many centers handling large numbers of facial palsy cases follow these guidelines closely [5, 36], there is great variation in how aggressively treatment is administered and whether physicians recommend optional treatments such as antiviral therapy and decompression surgery [5, 17]. For patients who retain loss of function or who develop aberrant regeneration, treatment options are limited to physical therapy, chemoderneravion of hyperactive muscles, and surgical reanimation[1-3].

1.2.8 CARE PROVIDERS

Patients presenting with BP often present in the emergency department or to their primary care providers [5, 7]. Often, these physicians will assume responsibility for treatment, though they may not be aware of current treatment guidelines. If referred to a specialist, BP patients may see a neurologist; while able to perform electrodiagnostics and provide standardized medical therapy (e.g. corticosteroid, antivirals, etc.), neurologists are not able to directly provide surgical treatment for BP. Otolaryngology (also known as otorhinolaryngology or ENT) is a more common specialty for referral of

BP patients, as these physicians are both familiar with cranial nerves disorders and are able to administer medical or surgical treatment during acute and chronic phases of BP. Many BP patients have their long term sequelae managed by otologists, a subspecialty of otolaryngology focusing on middle and inner ear and temporal bone pathologies, including pathologies of the facial (CN VII) and vestibulocochlear (CN VIII) nerves.

1.3 COMPRESSIVE MECHANISM

Inflammation is seen throughout the facial nerve in BP and has been reported both directly during autopsy and with MRI imaging [6, 37]. However, whether this inflammation produces sufficient compression of the facial nerve to induce neurapraxia is disputed. An understanding of facial anatomy, and specifically of the facial nerve, is needed to appreciate the proposed mechanical etiology of BP. The facial nerve leaves the middle cranial fossa and enters the skull at the internal acoustic meatus alongside the vestibulocochlear nerve (CN VIII), a narrow foramen that allows the two nerves (and their blood supply via the labyrinthine artery) very little room for expansion. After separating from the vestibulocochlear nerve and passing through the geniculate ganglion, the facial nerve makes a sharp turn within the skull and emerges from the stylomastoid foramen just beneath the ear. It is during its long course through the skull that the facial nerve is thought to be compressed from inflammation, and the site of compression is most often seen at the internal acoustic meatus [25]. Swelling-induced compression is postulated to cut off blood supply via the labyrinthine artery leading to conduction block. The severity and longevity of axonal damage is thought to be proportional to the degree of swelling [27]. However, no neural pressures have ever been reported during BP decompression surgeries, so the presence or absence of a compressive mechanism has been debated, as have the results of surgical decompression studies [6].

1.4 SURGICAL DECOMPRESSION

1.4.1 SELECTION CRITERIA

Because of the high spontaneous rate of recovery for patients exhibiting incomplete facial palsy, surgical decompression is only indicated in cases of complete facial palsy [7]. Though the symptoms of patients who will ultimately recover versus those who will

retain significant muscular impairment are indistinguishable upon onset of BP, the degree of conduction block has been shown to be a good predictive measure of future outcome [1, 25, 26]. Patients with less than 95% reduction in the peak amplitude of a suprathreshold evoked electroneurography (ENoG) compared to the unaffected side of the face almost universally have a spontaneous full recovery, while those with greater than 95% reduction have about a 50% chance of lasting moderate-to-severe muscular impairment. Thus, surgical decompression is recommended only to patients with complete facial palsy and whose electrodiagnostics demonstrate greater than 95% degeneration of the nerve and who demonstrate absent MUAPs on EMG testing.

1.4.2 SURGICAL TECHNIQUES

There are a number of different techniques for accessing the facial nerve directly through the temporal bone, each utilized in different clinical scenarios based upon the region of the nerve that must be accessed and the integrity of surrounding structures [38]. As summarized in Table 1, the five main surgical techniques for facial nerve exposure vary by approach and in facial nerve segments accessed, and thus are typically used for very specific applications. For Bell's palsy, the middle cranial fossa (MCF) approach has become the most common approach for decompression surgery by far, both because it accesses the two most physically constrained areas of the Fallopian canal – the internal acoustic meatus and the labyrinthine segment. The MCF approach allows visualization of the entire course of the facial nerve while minimizing the risk of injury to surrounding structures, unlike the transmastoid and translabyrinthine approaches which do not preserve the middle and inner ear. However, given the very small distances between vital structures within and surrounding the temporal bone (the middle and inner ear, dura, jugular vein, and carotid artery among them), extreme care and highly advanced surgical technique must still be employed with MCF decompression; the most common complications from MCF decompression are ossicular chain disruption resulting in conductive hearing loss, CN VIII or cochlear damage resulting in sensorineural hearing loss, vestibular dysfunction secondary to semicircular canal damage, and CSF leakage.

The surgical techniques employed for facial nerve decompression in the setting of Bell's palsy have drifted significantly since first performed in 1931 [26]. Early surgeons preferred the transmastoid approach, unaware the meatal segment was the most

common site of compression until this theory was proposed by Fisch and Esselen in 1972 [39]. Significantly improved patient outcomes were seen with meatal foramen decompression, and today MCF decompression is considered the safest method of facial nerve decompression in the setting of acute Bell's palsy [38].

Table 1: Summary of the five main surgical techniques used in facial nerve decompression, highlighting the segments of the facial nerve accessed and common indications or contraindications for each surgery.
GG: Geniculate Ganglion; AICA: Anterior Inferior Cerebellar Artery.

Approach	Segment(s) Accessed	Notes
Middle Cranial Fossa	Meatal, Labyrinthine	Most common in BP
Retrolabyrinthine	Pontine	AICA vascular decompression
Retrosigmoid	Pontine	AICA vascular decompression
Transmastoid	Tympanic, Mastoid, GG	Often lose incus
Translabyrinthine	All segments	Lose vestibulocochlear function

1.4.3 CLINICAL RESULTS

Early landmark studies conducted by Fisch in 1981 [25] and again by Gantz in 1999 [26] demonstrated clinically significant improvement in long-term functional recovery among patients presenting with severe Bell's palsy who underwent decompression surgery within 14 days of palsy onset. Subsequent studies have suggested surgical decompression is effective if performed anywhere between 3 days and 3 months post-onset [40-45]. In contrast, numerous other studies have found no significant difference between patients treated with surgical decompression and corticosteroid therapy compared to corticosteroid therapy alone [6, 46, 47]. As previously described, no comment is given on surgical decompression in the AAO-HNSF guidelines on treating BP because the clinical data surrounding its effectiveness is highly variable [7, 47]. Of these studies, most have examined differences among self-selecting cohorts of patients with widely varying times from onset to surgery and differing reliability in reporting of time and duration of onset. Variation among surgical techniques and functional recovery data acquisition and analysis has further confounded clinical results.

1.4.4 CONTROVERSY SURROUNDING DECOMPRESSION SURGERY

Decompression surgery is non-trivial, requiring bone manipulation in very close proximity to peripheral and central nervous tissue. Consequently, many physicians and patients are hesitant to encourage or undergo decompression surgery, especially early in the course of BP [5]. Among neurotologists, almost a third would not recommend surgical decompression even if a patient met established criteria indicating decompression, and half believe surgical decompression should not be standard of care [5]. 95% of neurotologists who perform surgical decompression perform fewer than one surgery a year, and over a third have not surgically decompressed the facial nerve in over a decade [5]. Thus, decompression surgery may be an underutilized mechanism of significantly reducing BP-associated morbidity because of our limited understanding of how the peripheral nerve responds to the decompression.

1.4.5 ANIMAL MODELS

To date, few animal models have been developed for studying the compressive component of BP. Mouse models based on HSV viral activation in the facial nerve have been developed, but have high failure rates (only 20% of mice inoculated develop facial paresis) and do not isolate the compressive mechanism from any effect from viral demyelination [48]. In addition, these models do not take into account the anatomical differences between the human and murine facial nerve during its course through the temporal bone, which is extremely important given the proposed mechanism of entrapment hinges upon unusually limited space within intratemporal canal. The most relevant model was conducted in 1972, when Hazama et al developed a rabbit model of compressive neuropathy on the facial nerve by applying a spring-loaded vice on the nerve, noting paralysis was instantaneous, unlike the gradual onset seen in BP, and could be reversed with increased blood pressure [49]. However, this model does not provide quantitative measures of the pressure applied to the nerve and likely is more simulative of transient ischemic attack rather than a progressive neuropathy with compressive mechanism. Additional animal models of entrapment neuropathies of the sciatic or median nerve have been described with approximate pressure quantification via blood pressure monitoring devices [50]. These models are extremely limited, however, in both their accuracy of pressure measurement and inability to be placed chronically. Prior devices for induction of entrapment neuropathies were designed for

large animals such as rabbits, and are not amenable to use in a high-throughput rodent model.

No prior device has been developed to quantify and study the long-term effects of cranial nerve compression in a live animal model. An animal model of the compressive mechanism of BP provides a mechanism to examine functional recovery due to purely decompression alone, not confounded by individual variations in immune system strength, rapidity in responding to viral reactivation, or skull morphology. A murine model permits functional recovery measurements by analyzing whisker motion amplitude and phase, a well-documented and widely accepted mechanism for assessing nerve recovery following insult [25].

1.5 STUDY AIMS

Because of the potentially neuricidal effects of viral reactivation and other genetic and environmental factors influencing the course of an individual's BP, as well as the inconsistent data in the literature, it is very difficult to isolate the role mechanical compression plays in functional loss. To date, no studies have characterized the relationship between facial nerve compression time and loss of facial function , nor the relationship between the timing of decompression and long-term recovery of facial function using a highly quantitative, reproducible animal model.

Furthermore, an animal model of the compressive mechanism of BP must provide a way to examine functional recovery due to purely compression in a randomized rather than observational manner. Such a model must also be unconfounded by individual variations in immune system strength, rapidity in responding to viral reactivation, skull morphology, or reporting of time and duration of palsy onset. A murine model is well suited to this task, with genetically and morphologically homogenous strains available. A rat model in particular also provides a quantitative mechanism for measuring functional recovery by analyzing whisker motion amplitude and phase, a well-documented and widely accepted mechanism for assessing faical nerve recovery following insult [51]. However, such a rat model still requires a method to induce consistent and reproducible pressure variations on a nerve.

Thus, this study aimed to (1) design, manufacture, and validate *in vivo* and *ex vivo* a fully implantable device that can induce a roughly physiologic pressure (circumferential and

gradually developing over ~24-72 hours) and measure this pressure in real time over the span of weeks to months, allowing quantitative comparison of pressure applied to a motor nerve to neural function, and (2) determine a pressure threshold at which Bell's-like phenomenon of facial nerve functional loss progressing over 24-72 hours occurs.

2 METHODS

2.1 DEVICE

The device built is open-source, simple to prototype, and inexpensive, and can be redesigned to accommodate acquisition of different types of data or implantation into different species of animals. For the purpose of collecting data pertinent to compression neuropathy of the facial nerve in a murine model, the device was designed to be fully implantable, able to induce a roughly physiologic pressure (circumferential and gradually developing over ~24 hours) on the marginal mandibular and buccal branches of a rat's facial nerve, measure this pressure real-time, and relay that pressure reading wirelessly from inside the rat to an outside receiver for analysis.

The device broadly consists of an implant and a datalogger that communicate wirelessly via radiofrequency. The implant takes *in vivo* temperature and pressure measurements and relays that that information to a datalogger. The datalogger receives information from the implant and stores it onto an SD card, which can then be analyzed and plotted as needed.

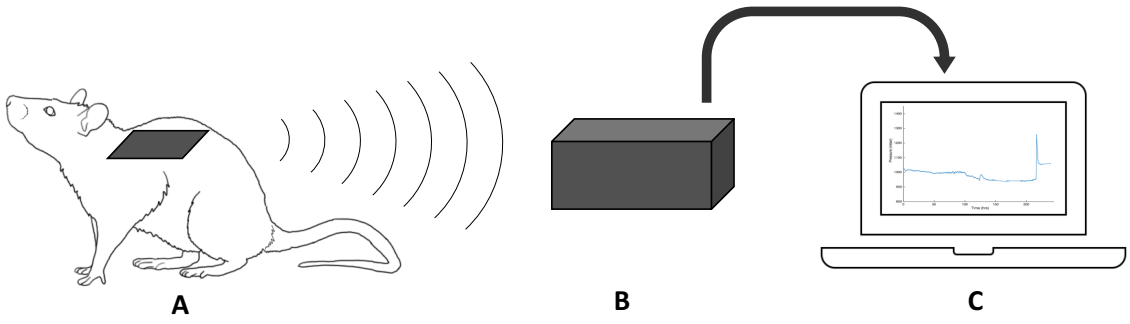

Figure 5: Workflow diagram showing implanted device (A) wirelessly transmitting data collected in vivo to a datalogger (B), which then logs the data for further analysis (C).

2.1.1 SOFTWARE AND CODING

2.1.1.1 IMPLANT

The implant consists of a microprocessor and pressure-temperature sensor integrated by printed circuit board (PCB). The entire implantable device measures 0.77in x 0.94in x 0.50in.

The microprocessor is a Simblee Bluetooth Smart Module RFduino (RFD77101 made by RFDigital), a miniaturized, wireless microprocessor that has the full functionality of an Arduino microprocessor board with radiofrequency transmission [52]. The entire Simblee is 7mm x 10mm x 2.2mm. The Simblee is programmed in the free, open-source Arduino coding environment. The scripts and libraries used for this device are included in Appendices 6.1 and 6.2.

The sensor used in the implant is a 2 bar waterproof pressure sensor, accurate to 2.5 mbar at physiologic temperature (MS5803-02BA) [53]. The sensor is ultralow power, operating on less than 1uA, and has an integrated analog-to-digital converter (ADC) that allows it to communicate with a microprocessor in I2C or SPI languages.

2.1.1.2 RECEIVER AND DATALOGGING

Another Simblee microprocessor acts as a receiver for the data broadcasted from the implant. The datalogger receives data from all implants as a character string, and stores this data, along with each implant's specific factory-assigned electronic serial number (ESN) and a timestamp (seconds since experiment start), to a comma-separated value file. It can additionally be recoded to store the data it receives to an external drive, such as an SD card, or directly to a computer, which can then be synced to the cloud for instant data access. When storing to an external drive, the receiver can be a wireless, miniaturized, portable device that can travel with an animal's cage. The Simblee microprocessor of the datalogger, like the Simblee on the implant, is programmed in the Arduino environment using a Simblee-specific command library. The code used to program the datalogger is included in Appendix 6.1.

The datalogger used in these experiments consisted of a Simblee rapid prototype module (RFD77201, RFDigital), a Simblee microSD shield (RFD22130, RFDigital), and a Simblee USB shield (RFD22124, RFDigital). The microprocessor on the rapid prototype module is programmed to constantly survey its airspace for any RF-transmitted payloads from other Simblee modules. Once receiving this payload in the form of a comma-separated character array, it writes the values to a comma-separated value (CSV) file on the microSD card. The receiver takes approximately 5ms to acquire a payload, and is unlimited in the number of devices it can receive from as long as these devices transmit 1ms or more apart. The receiver is powered by connecting it to a stable power source such as a wall outlet or computer via the USB shield, but can also be powered for shorter durations of up to 2 days using the Simblee battery shield powered by 2 AAA batteries (RFD22126, RFDigital).

2.1.2 HARDWARE DESIGN AND FABRICATION

The entire device was fabricated using commercially available products and vendors. The average cost was $220 per implantable device and $110 per datalogger. Calculations for this price estimate are included in Appendix 6.4.

2.1.2.1 PRINTED CIRCUIT BOARD

A printed circuit board (PCB) was created to minimize device space and integrate the microprocessor, sensor, battery, and other hardware. The PCB design (two layers, copper tracings, FR4 board) was created in the open-source PCB design software Eagle (Autodesk, Inc.) and printed using an outside vendor (Sunstone, Inc.). The board is powered by a CR1220 coin battery, and can be switched on and off remotely with a latched bistable magnetic reed switch (KSK-1E66) to conserve power during sterilization or between uses. Differential solder pads allow for switching between I2C or SPI communication as desired. Five vias corresponding to the five pins necessary to program the microprocessor (GND, VDD, Reset, Tx, and Rx) are included to temporarily connect the board to a computer for programming before disconnecting. This board could be redesigned easily to accommodate different sensors, microprocessors, or battery sizes. The electrical schematic for the board design is shown in Figure 6, and the full Eagle files of PCB schematic and board layout are included in Appendix 6.6.

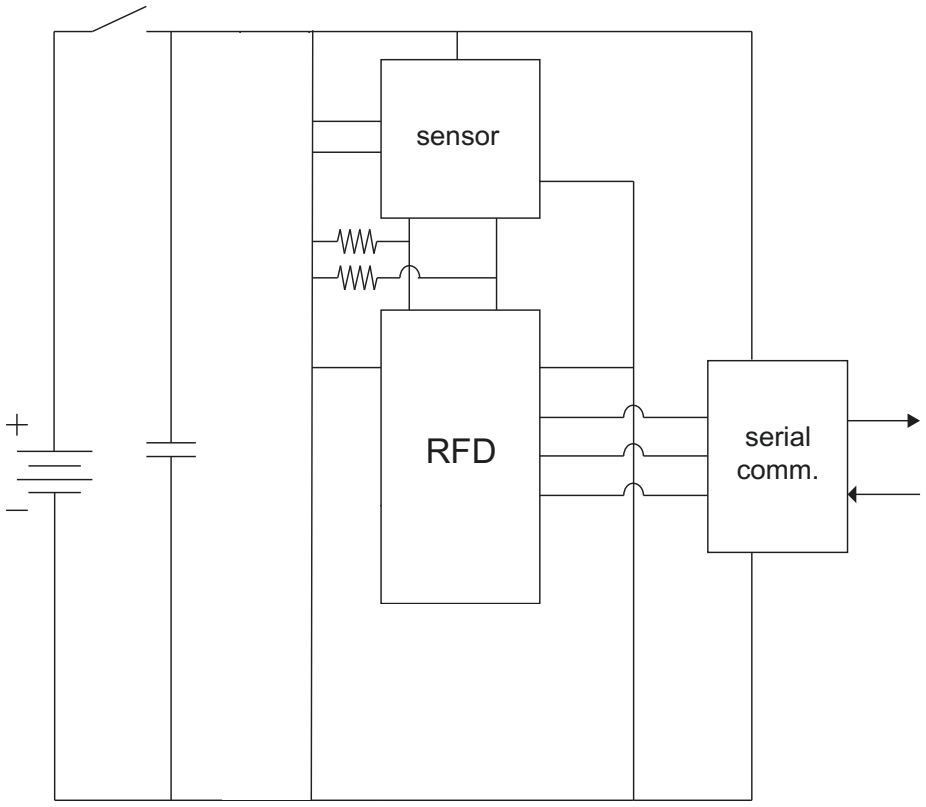

Figure 6: Schematic of printed circuit board, showing connections of Simblee microcontroller and sensor, as well as serial communication capability when connected directly to a computer via USB.

All components were soldered to the board using air reflow soldering and solder paste (ChipQuik Solder Paste). After solder paste was applied to the desired pins and all components placed appropriately, the PCB was suspended over 110°F air with local application of 570-590°F air jet over the component being soldered to induce solder paste melting.

2.1.2.2 ASSEMBLY WITH CUFF AND INJECTION PORT

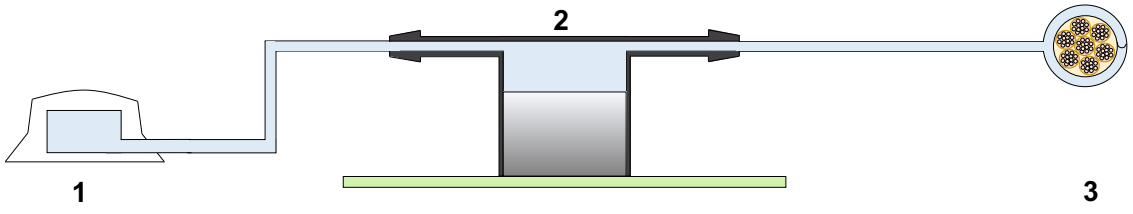

Figure 7: Diagram of connections between injection port (1), 3D printed fitting (2) overlying sensor (gray) and PCB (green), and occlusion cuff (3) surrounding nerve (orange). Fluid (blue) can flow freely between the port, sensor, and cuff.

The cuff for nerve occlusion (Vascular Occlude Cuff, Access Technologies) is designed to have a continuous lumen with the sensor and a subcutaneous injection port (Rat-o-port, Access Technologies) such that pressure can be dynamically altered and measured while the cuff is implanted *in vivo*. A custom fitting to transition from the sensor diameter to the much smaller cuff diameter was designed in SolidWorks and 3D printed (Appendix 6.7). The connections of the cuff, injection port, and sensor are shown in Figure 7, and images of all assembled components are shown in Figure 8.

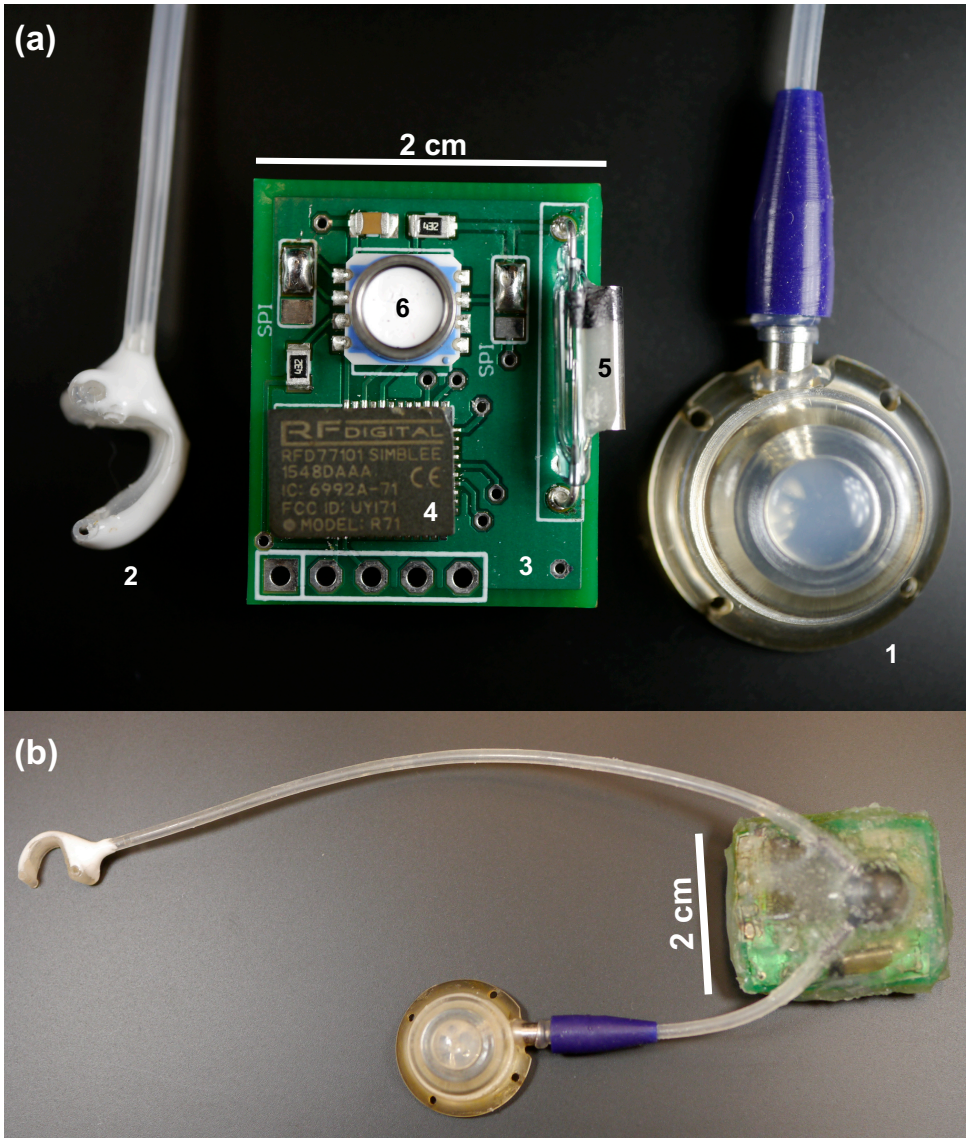

Figure 8: (a) Implant deconstructed without silicone encasement, showing (1) subcutaneous injection port, (2) hydraulic cuff, (3) printed circuit board with (4) microcontroller (Simblee), (5) magnetic switch, and (6) pressure sensor. (b) Implant with parts assembled and encased in silicone.

2.1.2.3 DEVICE POTTING AND SILICONE COATING

To be implanted, the device need to be coated in a medical-grade, biocompatible material – for this purpose, medical-grade silicone (A-103, Factor II, Inc.) was chosen. However, completely potting the device in silicone made the device heavy (density [ρ] = 1.1g/cm^3) and did not completely waterproof the board given the material's semipermeability to water and prolonged device exposure to serous fluid while implanted. Thus, the entire device was first potted in epoxy (Loctite Instant Mix Two-Part Epoxy Quick Set^{TM}) to completely waterproof the board and minimize device weight (ρ < 1.0g/cm^3).

The epoxy-coated board was subsequently coated with 2-3mm of medical-grade silicone. The silicone, formed of a 1:10 weight-based combination of curing agent to elastomer (A-103, Factor II, Inc.), was mixed and defoamed for 2 minutes at 2000 rpm in a planetary mixer (ARE-310, Thinky Mixer USA) before pouring. To minimize weight, the silicone could be poured over the epoxy-coated device while suspended in a vice, allowing excess silicone to drip off the edges of the device. Once poured, the silicone was cured at room temperature to avoid battery damage experienced with heat application. The final device, once potted and coated in silicone, measured approximately 20mm x 30mm x 15mm and weighed 10g.

If a thicker layer of silicone was desired, the silicone could instead be applied within an acrylic jig, which was composed of layers of laser-cut acrylic stacked to provide flexibility in final device height The jig was custom-designed in Adobe Illustrator and cut with a CO2 laser cutter. The jig was designed to accommodate the board with 3-4mm of space for silicone on all sides. Indentations within one layer of the jig created tracks for the device tubing to exit the jig without being compressed. Small silicone phalanges were also designed into this layer for securing the device to surrounding tissue during surgery. Compressive force to prevent the acrylic layers from separating was provided with screws through the corners of the jig spanning all layers. The specifications of the jig layers are further defined in Appendix 6.8. When using the jig, an initial layer of silicone 1-2mm thick was then poured into the base of the jig and partially cured with hot air gun for 30-60 seconds. Once cooled, the device was placed into the jig and silicone was poured over the entire PCB, custom fitting, and all tubing joints.

2.1.2.4 DEVICE STERILIZATION

To sterilize before implantation, the entire silicone-coated device was sterilized with ethylene oxide (Massachusetts General Hospital). The implants were then put under vacuum for 5 days to remove ethylene oxide from the silicone and prevent leeching into tissue after implantation. Notably, autoclaving the devices is possible but significantly reduces battery life, and 12mm heat-resistant coin cell batteries are unable to provide the necessary current for wireless data transmission – however, this device could be autoclaved if modified to accommodate an alternate battery source.

2.1.3 SURGICAL IMPLANTATION

2.1.3.1 HEADFIXATION

Female Lewis rats aged 65-90 days were anesthetized with isoflurane (3.5% during induction, 2% during operation) until unresponsive to toe-pinch. A 2 cm incision was then made midline over the calvarium down to the bone and the bone exposed with the galea scraped off with a scalpel. A percutaneous titanium head-fixation device was affixed to the calvarium with titanium screws. The incision was then closed primarily with a running 5-0 Vicryl suture. Once the procedure was complete, isoflurane was removed and the rats were allowed to recover under observation until moving normally within their cages. Rats were treated with topical antibiotic (Bacitracin Zinc) on the incision sites and eyes. Post-operative pain was managed with meloxicam (0.1mL/100g bodyweight subcutaneous injection) every 24 hours for 48 hours. Rats were allowed to recover for 2 weeks postoperatively without handling.

2.1.3.2 DEVICE IMPLANTATION

Lewis rats previously implanted with a percutaneous titanium head-fixation device were anesthetized with isoflurane (3.5% during induction, 2% during operation) until unresponsive to toe-pinch. A 1.5cm superficial cut through only the dermis and superficial musculoaponeurotic system (SMAS) was made over the left cheek and the buccal and marginal mandibular branches of the facial nerve (innervating the whisker pad) were identified with bipolar electrical stimulation. Both branches were fully cleared such that the two branches could be brought together without tension (Figure 9a). A

pocket large enough for the body of the PCB and injection port was made on the rat dorsum centered over the scapulae. The cuff of the device was tunneled from this pocket to the device and wrapped around the cleared buccal and marginal mandibular branches and closed with a suture (Figure 9b), and the device tacked in place to skin and superficial latissimus muscles by throwing a mattress suture through each of two silicone phalanges extending from the implant. The incisions on the face and back were then closed primarily with a running 5-0 Vicryl suture. Once the procedure was complete, isoflurane was removed and the rats were allowed to recover under observation until moving normally within their cages. Rats were treated with topical antibiotic (Bacitracin Zinc) on the incision sites and eyes. Post-operative pain was managed with meloxicam (0.1mL/100g bodyweight subcutaneous injection) every 24 hours for 48 hours. Baseline measurements of nerve function before pumping up were taken before surgery and 3 days post-operatively to ensure no functional damage ensued from surgical manipulation.

Figure 9: ***Surgical device implantation:*** **(a) The cuff and device in place before suturing closed, showing device sitting in pocket above scapulae and cuff tunneled through to whisker pad incision. (b) Placement of the cuff around the marginal and buccal branches of the facial nerve. (c) Animal 3 days post-operatively with implant visible on back.**

2.1.4 WHISKER MOTION ANALYSIS

Lewis rats previously implanted with a percutaneous titanium head-fixation device at least two weeks status-post surgery underwent an additional two weeks of daily manual conditioning to tolerate human handling and gentle restraint in a cloth sack necessary for whisker motion tracking and analysis.

Whisking analysis was completed using two different whisker tracking systems. From 2016-2017 whisker motion was tracked with laser micrometer-based system as described by Heaton et al., and from 2017 - 2019 whisker motion was tracked with a

video tracking-based system, as described by Guarin, et al[54, 55]. Using the laser micrometer-based whisker tracking, whisker amplitude during protraction (forward motion of the whiskers relative to the whisker pad) and retraction (rearward motion of the whiskers relative to the whisker pad) was monitored for a duration of 5 minutes. Whisker motion of the right and left sides was tracked independently. Function of the right and left facial nerves was quantified as the average of the amplitude of the 3 largest whisking motions on the right and left, respectively. Relative function of the affected and unaffected sides could thus be determined as the ratio of the mean of 3 maximum whisks on the affected (left) and unaffected (right) sides. The design, setup, and signal processing behind this system is explained in greater detail in Heaton, et al. [54].

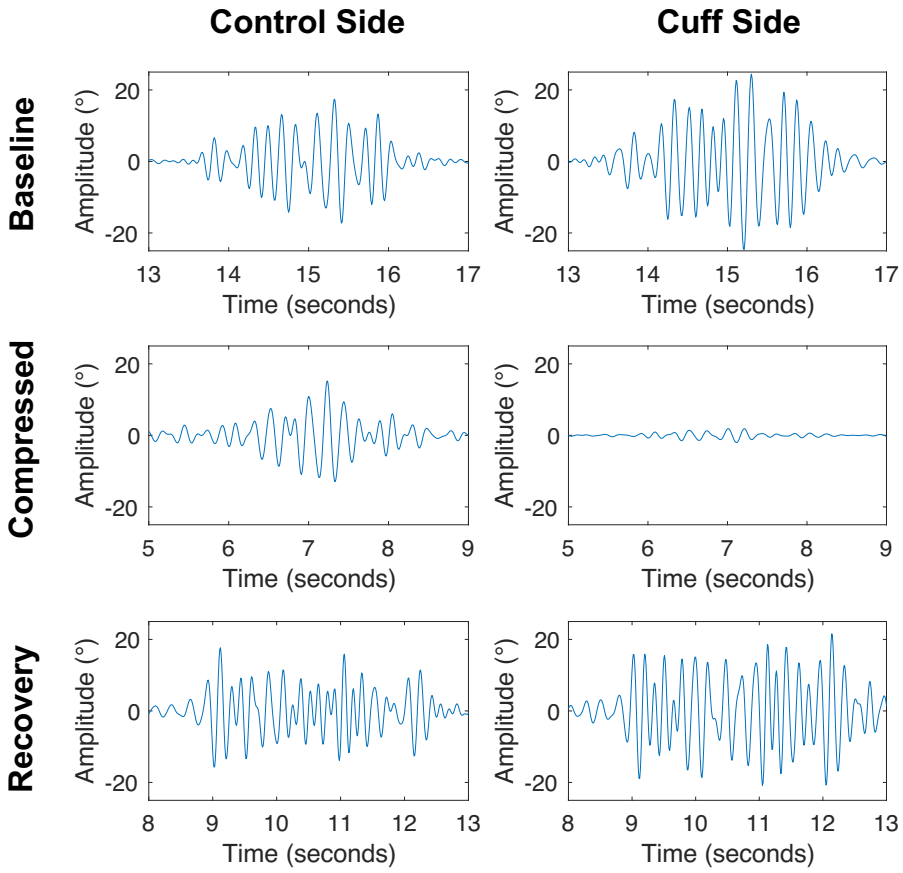

Figure 10: Isolated period of whisking plotted after post-processing, with demonstration of whisking motion at baseline (top), while compressed (middle), and after recovery from compression (bottom).

Using the video-based whisker tracking, whisker position was tracked frame by frame with images taken from a 500 frames-per-second (fps) camera. Images from the camera were first converted to a series of black-and-white Tagged Image File Format (TIFF)

images that were then downloaded into RatVideoAnalysis, an open-source Python-based program that allows the user to identify the rat's whiskers, eyes, and a region of interest (ROI) in which the whiskers will move. The program then automatically tracks right- and left-sided whisker motion independently as x- and y-coordinates in space, and can export and plot these points to graphically represent the whisker motion waveform. Representative whisks of a healthy, damaged, and recovered nerve tracked using this system are demonstrated in Figure 10. Once the waveform is established for both sides, the data was imported into MATLAB and a low-pass filter was applied to remove any signal from outside of the rat's reported frequency of whisking (0-20 Hz)[55]. Defining a whisk as any local maximum at least 50% that of the maximum-amplitude whisk, the mean of all whisks was computed for both sides. Similar to the prior micrometer-based system, relative function of the affected and unaffected sides could subsequently be determined as the ratio of the mean amplitude of the affected (left) and unaffected (right) sides. The design, setup, and signal processing behind this system is explained in greater detail in Guarin, et al.[55]. The code used to filter and process the data is included in Appendix 6.4.

2.1.5 FACIAL NERVE PRESSURE THRESHOLD DETERMINATION

Determination of the required pressure at which to induce a Bell's-like phenomenon was done in a step-wise process, with the results of a "coarse search" over a broad range of pressures directing a "fine search" in a more narrow range of pressures. The first study "coarse search" study consisted of a single rat used as a proof of concept to determine a minimum pressure threshold at which no functional loss was seen and a maximum pressure threshold at which total functional loss was seen rapidly (i.e. within 24 hours). After this study, a larger "fine search" study with 3 rats was used to determine a precise pressure range (within 50 mmHg) at which functional loss was seen.

2.1.5.1 COARSE MINIMUM AND MAXIMUM PRESSURE THRESHOLD DETERMINATION

A Lewis rat previously implanted with a percutaneous titanium head-fixation device and conditioned to tolerate rigid head restraint to enable recording of whisking activity while awake was first tested for baseline whisker function. The rat was then implanted with a device filled with normal saline to 0 mmHg above atmospheric pressure and allowed to

recover for seven days postoperatively. On postoperative day (POD) 7 a second baseline whisker function was recorded to assess for any functional loss due to trauma during implantation. After this, the device was pumped up to approximately 50% maximum systolic blood pressure (75 mmHg) using injection of 0.02 mL of 10% glycerol solution for 8 days, with whisker function recorded daily. After 8 days of low-pressure facial nerve compression (POD 15), the device was pumped up to approximately 400% maximum systolic blood pressure (600 mmHg) using injection of 0.02 mL of 100% glycerol solution for 8 days, with whisker function recorded daily. After an additional 8 days of high-pressure facial nerve compression (POD 23), the device was surgically removed to simulate decompression surgery. Whisker function was then recorded every 4 days for a total of 28 days (through POD 50). Upon study termination, the rat was euthanized.

2.1.5.2 FINE MINIMUM AND MAXIMUM PRESSURE THRESHOLD DETERMINATION

Three previously headfixed and sack-trained Lewis rats were tested for baseline whisker function. Each rat was then implanted with a device filled with normal saline to 0 mmHg above atmospheric pressure and allowed to recover for 3 days postoperatively. On postoperative day (POD) 3 a second baseline whisker function was recorded to assess for any functional loss due to trauma during implantation. After this, the devices were pumped up in each rat to different goal ranges – a low-pressure range of 0-100 mmHg above atmospheric, a medium-pressure range of 200-300 mmHg above atmospheric, and a high-pressure range of 300-500 mmHg above atmospheric. Pressures were initially attained with injection of 0.01-0.03 mL of 50% glycerol solution, with the goal to be in the low end of the pressure range initially and slowly rise over time. Injection of additional 0.01-0.02 mL of 50%-90% glycerol solution or fluid withdrawal via the port were performed as needed to maintain pressure within the desired range.

After 5 days of compression within the target range (POD 8), the device was surgically removed to simulate decompression surgery. Whisker function was then recorded daily for 7 days after decompression, and then weekly after that for 6 weeks (through POD 54). Upon study termination, all rats were euthanized.

2.1.6 HISTOLOGY

2.1.6.1 TISSUE PROCESSING

Immediately following CO2 euthanasia in accordance with institutional animal care protocols, rats were transcardially perfused with 4% phosphate-buffered paraformaldehyde (PFA). Left facial nerves were harvested and post-fixed by immersion in 4% PFA for 48h, followed by cryoprotection in 30% sucrose for 24h. Each harvested facial nerve was sharply divided into three segments: proximal, lesional (in the area of compression), and distal, prior to cryosectioning at 5 µm, and staining with Fluoromyelin Green (1:300, Molecular Probes, Eugene, OR) for confocal microscopy, similar to previously described methods [56, 57].

2.1.6.2 TISSUE IMAGING

Confocal images were collected with a Leica SP8 (Leica Microsystems) confocal microscope equipped with a resonant scanner and 64X (1.3 NA) oil objective lens. FluoroMyelin (Molecular Probes) green was excited with a 488 nm Argon laser. Fluorescent signal was collected at 550/50 nm (FluoroMyelin green) using Leica HyD hybrid detectors controlled with the Leica Application Suite X software. Proprietary deconvolution software, Lightning (Leica Microsystems), was uniformly employed for enhancement of image quality. For all images, brightness and contrast were adjusted for better visualization (identically for compared image sets) using Fiji ImageJ software, Version 1.52e [58].

3 RESULTS

3.1 EX VIVO VALIDATION

The implant was assessed both *ex vivo* for basic data measurement accuracy and implanted in a series of animals to demonstrate functionality *in vivo*.

3.1.1 PRESSURE VALIDATION

Given the device is required to both detect change in pressure and hold a constant pressure reading over time, validation of dynamic and static pressure measurements

was performed. Pressure readings from the implant were directly compared to values from an analog pressure regulator.

For dynamic pressure measurement validation, the implant was exposed to a rapid increase and decrease in pressure of 350 mmHg (from atmospheric pressure of 1000 mbar to 1500 mbar), approximated by a square wave. As shown in Figure 11a, the sensor was very sensitive to rapid pressure changes and settled to an accurate and stable pressure reading within less than one second.

For static pressure measurement validation, the implant was exposed to a constant 300mmHg above atmospheric pressure (1400 mbar) over the course of 6 days (Figure 11b). Demonstrated in Figure 11c, the sensor was able to hold a very stable and accurate pressure reading during this time, with maximum pressure variation recorded as 20 mmHg (25 mBar).

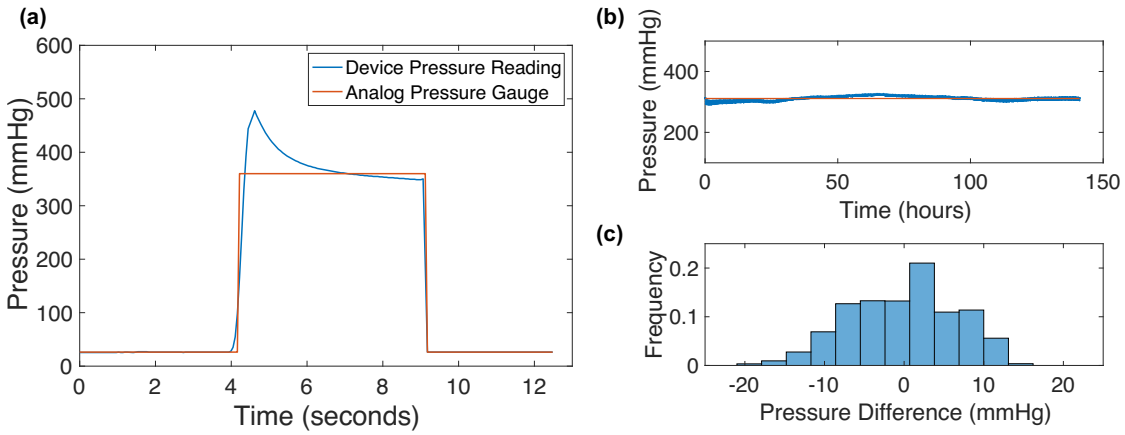

Figure 11: ***Validation of device pressure sensor (shown in blue) against analog pressure gauge (shown in orange).*** **(a) Dynamic pressure monitoring shows return to baseline within two seconds of rapid pressurization. (b-c) Static pressure monitoring held over multiple days (b) shows error less than 20mmHg from analog pressure values (c).**

3.1.2 CUFF PRESSURIZATION

Because the model for inducing compressive neuropathy relies upon a precise way to induce and maintain pressure within the occlusion cuff, a deeper understanding of the dynamics of cuff pressurization was needed.

3.1.2.1 PRECISION CUFF PRESSURIZATION

As implanted devices were programmed to transmit relatively infrequently (e.g. on the order of once per hour) to conserve battery while implanted, the final pressure achieved immediately after injection of fluid into the injection port is not relayed by the device in real time. Because of this, a mechanism for remotely measuring the pressure within the device with a high sampling frequency during and after pressurization was required. To accomplish that, a remote pressure monitor was built by connecting a second device, programmed to transmit pressure continuously, to a syringe. Diagrammed in Figure 12a is the connection between the sensor and syringe, highlighting the ability for fluid to move continuously between the device and the remote pressure monitor via a hypodermic needle attached to the syringe.

However, because of the viscosity of the fluid injected and the very narrow caliber of the hypodermic needle, rapid pressure equilibration between the monitor and the device is not guaranteed. To validate that the remote monitor can be an accurate measure of the pressure within the device, the pressures relayed by the remote monitor was compared to an *ex vivo* device set to transmit continuously. As shown in Figure 12b, a large-bore needle (18 gauge) was necessary to allow for temporally and mechanically accurate measurements of the pressure within a device to the pressure measured with an outside monitor. However, there were a number of difficulties using this type of remote pressure monitor *in vivo*. While possible to utilize such a large needle a rat, it is more painful for the animal than using a small-bore needle, requiring temporary sedation to pump up the device. Additionally, repeated usage of a large-bore needle damages the integrity of the injection port, reducing the lifespan of these devices. However, the largest obstacle to using a remote pressure monitor to detect the pressure within the device was because of the cuff permeability to water, resulting in significant change in cuff pressure within the 12-24 hours after pressurization, obviating the need for precise real-time measurement of the pressure within the device at the time of injection. For these reasons, a remote pressure monitor was abandoned with the device as currently fabricated, but could be utilized with a different device that does not use semipermeable cuffs.

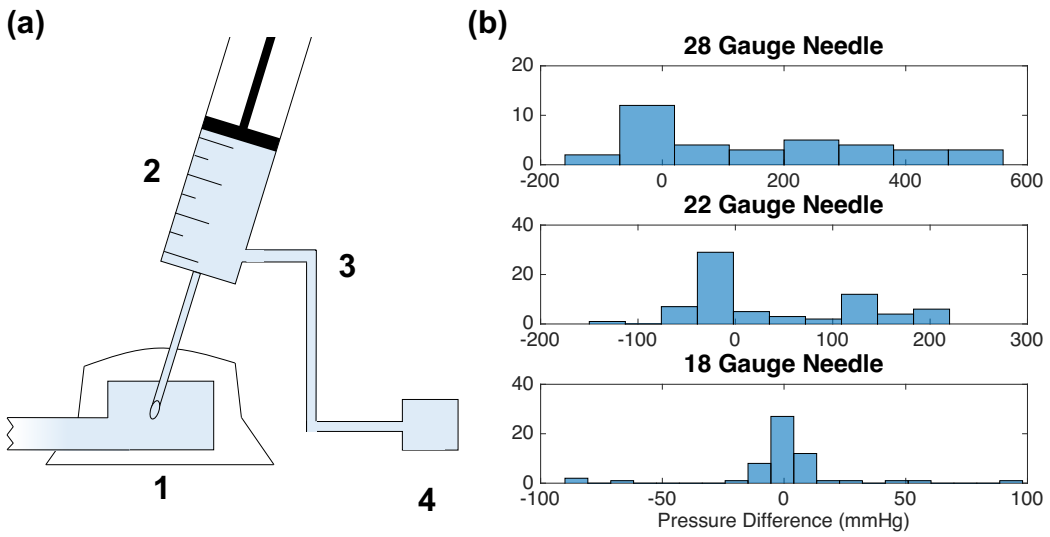

Figure 12: ***Monitoring of pressure injected into port remotely.*** **(a) Diagram of the remote pressure monitor. Highlighted in blue is the continuous path between the (1) implant port, (2) syringe, and (3) tubing connecting to the (4) monitor sensor. (b) Difference between remote pressure sensor and device pressure reading with different sizes of needles, showing concordant pressures between implant and monitor within 10mmHg when using a wide-bore needle (18G), but with increasingly discrepant readings with smaller needles. Variation between monitor and implant pressures was seen transiently with pressure changes, but stabilized within 1-2 seconds, as shown in Appendix 6.9.**

3.1.2.2 ONCOTIC PRESSURE-DRIVEN CUFF PRESSURIZATION

The silicone cuff is air and water permeable; thus, pressurization with air or normal saline was impossible due to rapid depressurization, and the tonicity of the fluid injected must be taken into account to prevent undesired pressure changes *in vivo* (Figure 13a). In this way, oncotic pressure dictated the final pressure achieved in the cuff. However, the permeability of silicone is based upon spaces between crosslinks within the material (roughly approximated as pores) – while well characterized in the literature, is very difficult to predict pore size, and thus permeability, in a dynamic system, as it is affected by material manufacture, temperature, and pressure[59, 60]. At least two of these variables apply to the devices directly; (1) the cuffs are commercially made and thus not necessarily adherent to a particular permeability constraint by the manufacturer, and (2) the wide pressure variation induced in the cuff stretches the silicone and thus increases its porosity, thereby changing its permeability. Given the complexity of modeling this system, empiric understanding of the changes in pressure of each cuff in response to hypertonic injection was necessary.

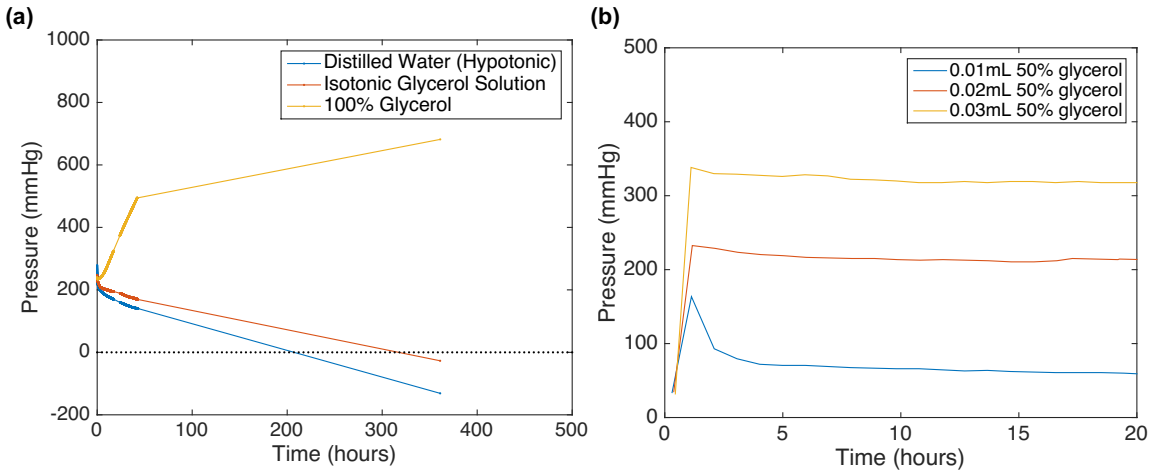

Figure 13: ***Change in pressure within cuff as a function of tonicity.*** **(a) Cuffs pressurized to the same value show drop below atmospheric pressure with hypotonic solution (blue), return to atmospheric pressure with isotonic solution (red), and increase in pressure with hypertonic solution (yellow). (b) Different final pressures achieved with injection of varying amounts of 50% glycerol solution in normal saline, which results in different final glycerol concentrations in the cuff given constant starting volume for all three trials.**

Glycerol was chosen because of its high molecular weight, water solubility, biological inertness, and extensive characterization for biological systems[61]. When implanted, the cuff was filled with normal saline. When pressurized the port was injected with hypertonic glycerol solution; in this way, oncotic pressure into the cuff would balance hydrostatic pressure out of the cuff, maintaining the pressure inside the cuff at a steady, elevated pressure. Notably, the cuff did need to be pressurized above atmospheric to achieve a change in pressure – this is likely due to the pressurization stretching the cuff enough to induce a meaningful increase in pore size, and thus in permeability of the silicone cuff.

3.1.2.3 CHARACTERIZING FLUID MIXING WITHIN TUBING

Mixing of fluid within the tubing is governed by a combination of diffusion and turbulent mixing. Turbulent motion occurs with excess externally-applied kinetic energy, when shear forces between fluid particles exceeds the damping forces of particle-to-particle interactions determined by the fluid's viscosity and thus transitions the fluid's motion from laminar flow to turbulent flow. Thus, turbulence is a very rapid form of fluid mixing that occurs on the order of milliseconds – seconds. Diffusion, however, results from the random Brownian motion of individual particles within a solution that is determined by the kinetic energy attributed to each particle. Though this is governed by both intrinsic

factors (e.g. solution composition) and extrinsic factors (e.g. solution temperature), it is a very slow process that, in the absence of additional turbulent mixing, is usually only significant at length scales of micrometers or less. In this system, with the length of the tubing being on the order of centimeters, pure diffusive mixing has negligible impact.

Reynolds number (Re) approximates the relative contributions of inertial and viscous forces in fluid flow, and can be used to determine if fluid dynamics in a particular environment will remain laminar (Re < 2100) or will progress to turbulence (Re > 4000), and thus include turbulent mixing. Reynolds number is calculated as

$$Re = \frac{\rho v L}{\mu}$$

where ρ is the fluid density, v the fluid velocity, L the characteristic linear dimension (for a pipe this is diameter), and μ the dynamic viscosity of the fluid. For this system, the tubing diameter (L) is $1x10^{-3}$ m, the dynamic viscosity of pure glycerol (μ_g) is 0.91 Ns/m^2, the dynamic viscosity of water (μ_w) is 8.9 x 10^{-4} Ns/m^2, the density of pure glycerol[2] (ρ_g) is 1258 kg/m^3, and the density of water (ρ_w) is 997 kg/m^3. While no direct measurement of fluid velocity can be used in this calculation, using a Reynolds number of 2100 we find that pure water and pure glycerol would have to be moving 1.9 m/s and 1.5 x 10^3 m/s, respectively, to achieve any non-laminar turbulent flow in this system, which is much faster than any fluid velocity achieved with injecting even pure distilled water[3]. Thus, it can be expected that all fluid mixing with injection alone would rely upon diffusion, which is far slower than the 48-72 hours of pressurization desired to mimic a Bell's Palsy-like phenomenon. Thus, because of this, external mixing within the injection syringe needs to be performed to ensure adequate mixing of any fluid within the cuff with fluid being injected into the system.

This was validated in a device ex vivo by injecting food coloring into a device already filled with saline. As is shown in Figure 14, the food coloring does not advance into the

[2] While precise calculation of the density of a glycerol:water mixture is subject to a contraction coefficient, this coefficient is negligible under the conditions assumed, as described in Volk et al. [61]

[3] Maximum possible velocity would be to fill the entire tubing system to the cuff (~15cm) within the minimum human reaction time (for this writer ~0.1 seconds), which would translate to a velocity of 1.5m/s and a Re for water of 1680.

cuff unless mixed manually within the syringe, but once mixed is homogenously mixed throughout the system including into the distal ends of the cuff.

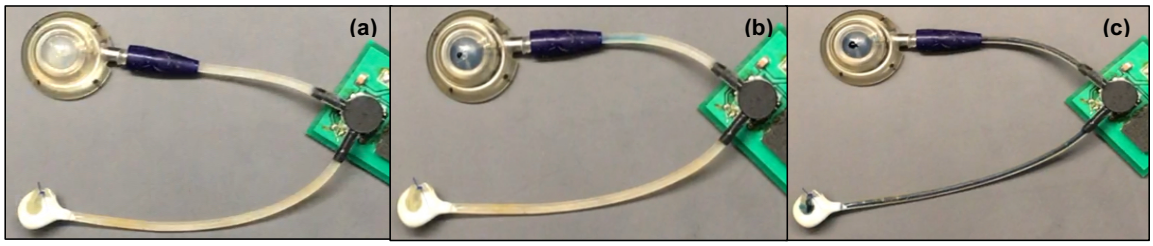

Figure 14: Food coloring injection into port and cuff filled with saline, showing (a) pre-injection device filled with saline, (b) device 10 seconds after injection of 0.5mL food coloring into port, showing incomplete filling and no mixing of food coloring and saline, and (c) device after 3 fluid withdrawals and reinjections with the syringe, showing food coloring mixed well into the distal ends of the occlusion cuff.

3.1.3 DEVICE LIFESPAN

Device lifespan was assessed by tracking time to failure for devices programmed to transmit a data payload every hour. It was found that devices transmitting their voltage had significantly decreased lifespan of approximately 24-48 hours with a CR1220 battery (40mAh, 12 mm diameter, 0.9g), and approximately 150-200 hours (approximately 1 week) with a CR2032 battery (235 mAh, 20 mm diameter, 2.8g). However, when removing the voltage monitoring, the device could run more than 9 weeks continuously transmitting once per hour on a CR1220 battery, which is more than two times the necessary device lifespan (based on 21 days as the furthest timepoint at which neural decompression surgery is recommended in humans).

3.1.4 PAYLOAD SIZE LIMIT

No documentation was available on the maximum payload size that could be transmitted wirelessly while operating in SimbleeCOM mode. To determine this limit, a Simblee was programmed to repeatedly send payloads, increasing the payload by one bit each cycle. A payload of 15 bits was found to be the maximum, and payload of greater than 15 bits result in sending a repeating cycle of 3-4 old payloads. Care must therefore be taken to avoid sending a payload greater than 15 bits, as this signature repetition cycle is often difficult to detect.

3.2 IN VIVO VALIDATION

3.2.1 DEVICE IMPLANTATION

The implanted devices were well tolerated, showing no signs of extrusion or irritation over multiple weeks of implantation. Data transmission was reliable throughout the course of implantation, and hourly data from multiple animals in the same room was collated by a single datalogger without missed datapoints.

3.2.2 COARSE MINIMUM AND MAXIMUM PRESSURE THRESHOLD DETERMINATION

Figure 15 shows the overlaid data of facial nerve function (as percent relative maximum whisking amplitude between compressed and non-compressed sides) and cuff pressure (mmHg) over three weeks of implantation and seven weeks of functional monitoring. No functional impairment was seen through 10 days after implantation of the unpressurized cuff. The low-pressure study showed no functional impairment throughout the eight days of compression at a pressure of 70 mmHg. The high-pressure study subsequently showed immediate complete functional loss at the maximum threshold pressure of 600mmHg that was maintained throughout the eight subsequent days of compression. After release of maximum threshold cuff pressure and device explant, whisking function improved to approximately 50% of baseline. Notably, there was difficulty maintaining an adequate seal between the device's 3D printed fitting and the board at the time of the study due to constraints in manufacturing. Thus, the high pressure induced on POD15 resulted in the 3D printed part shearing off of the printed part and leaking fluid from the cuff and port onto the board, shorting it and eliminating further data transmission. Thus, pressure data from POD15 – POD23 was graphically represented with a dashed line to indicate this data was presumed to be the last known pressure from the device, but could have fluctuated significantly within that timepoint.

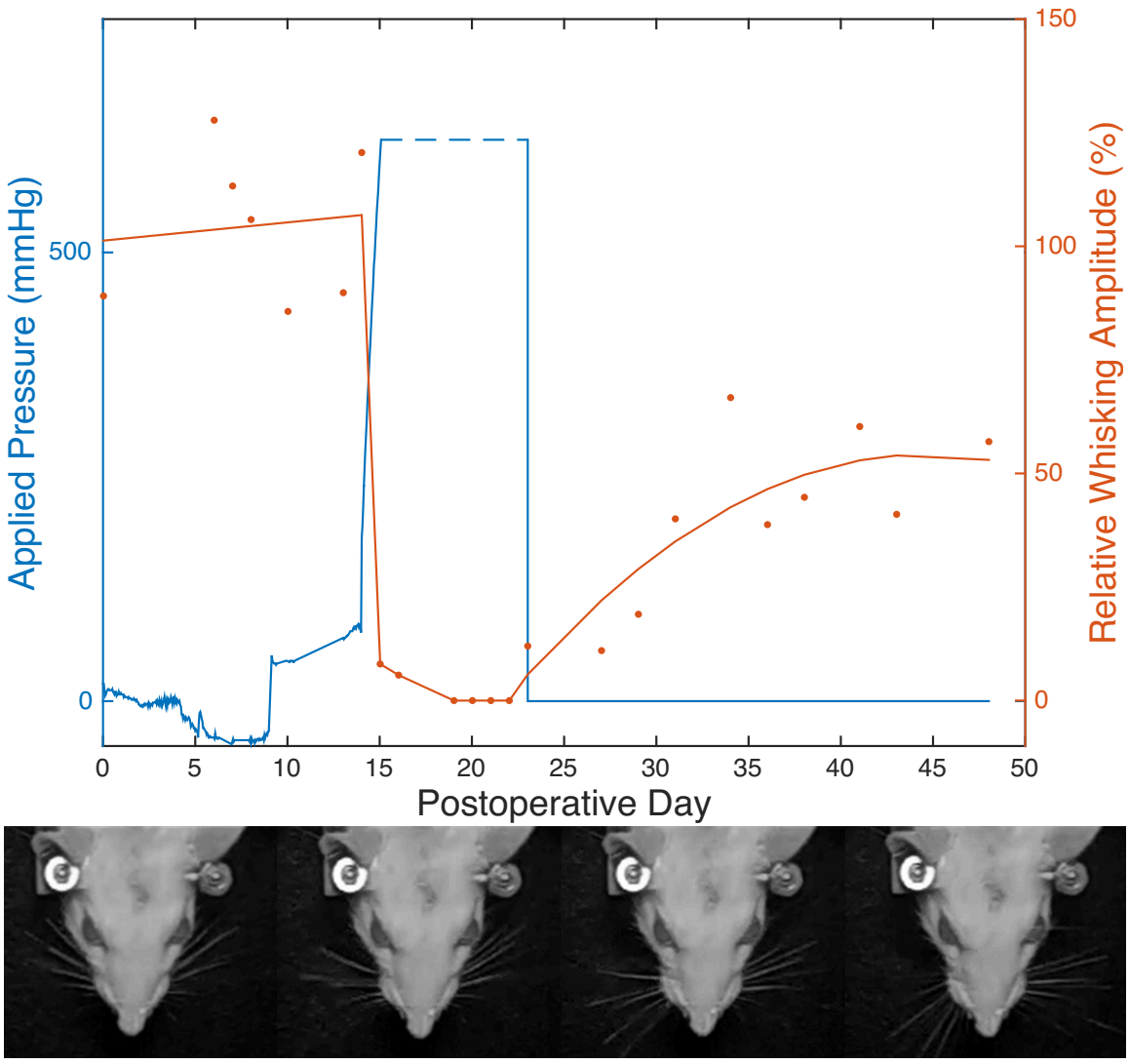

Figure 15: ***Functional loss and recovery with cuff insufflation and deflation.*** **Top: Relative maximal whisker displacement between implanted (left) and normal (right) sides, displayed together with cuff pressures (above atmospheric) as a function of time (postoperative day, POD). Lack of functional loss up to POD 15 following implantation at atmospheric and low (50 mmHg) applied cuff pressure is demonstrated. Immediate and complete loss of function is seen with high (625 mmHg) applied pressure (POD 15), sustained throughout 8 days of pressure application. A gradual return of whisker function up to ~50% of normal was noted in the days following deflation of the cuff (POD 23) to atmospheric pressure (PODs 23-50). Bottom: Whisk sequence captured with high-speed camera of animal on POD 50, demonstrating impaired whisking on left side (previously implanted), with normal right-sided whisker function.**

3.2.3 FINE MINIMUM AND MAXIMUM PRESSURE THRESHOLD DETERMINATION

As shown with the overlaid functional and pressure data in Figure 16, the low-pressure range resulted in no functional loss across all 5 days of compression. The rat held at 300-500 mmHg immediately (within 24 hours) demonstrated complete functional loss once pressure was brought above 300 mmHg, and demonstrated only partial facial nerve recovery to approximately 50% by 6 weeks post-decompression. The rat held at 200-300 mmHg, however, showed no loss of function until the pressure reached 250 mmHg, at which point facial nerve function slowly declined to < 50% over the course of 72 hours; subsequent decompression the following day resulted in complete recovery of within 48 hours. Of note, the rat held at medium pressure (200-300 mmHg) was not tested at timepoints further than POD 32 because of titanium head-fixation device extrusion from the skull resulting in the animal experiencing pain during testing. However, given this rat had already returned to baseline nerve function on the compressed side, further testing was deemed unnecessary.

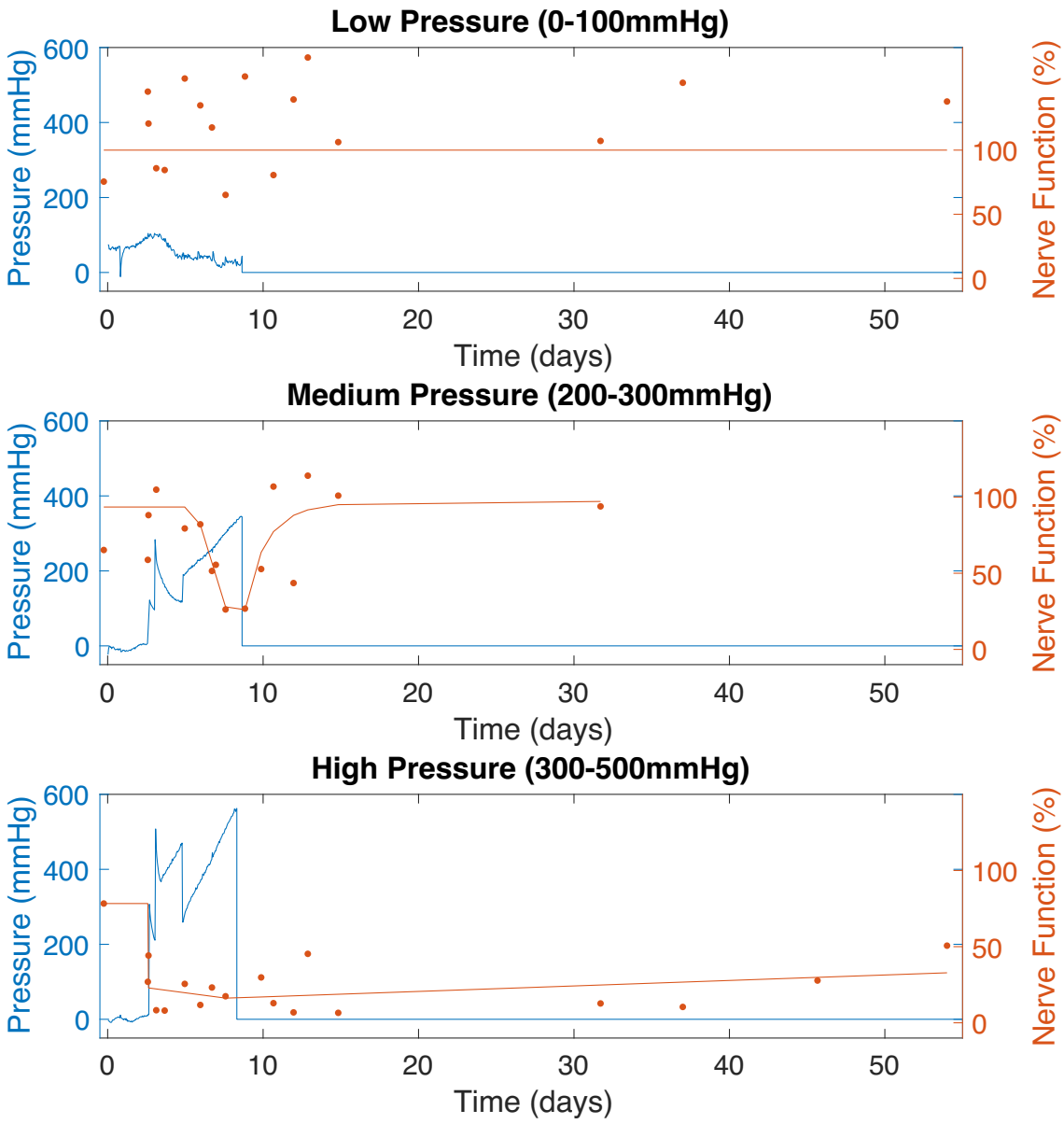

Figure 16: ***Comparison of compressive pressure and function over varying applied compressive forces.*** **Shown in blue are the pressures read from each rat every hour, held at low (0-100mmHg), medium (200-200mmHg), and high (300-500mmHg) pressure ranges. Shown in orange is the nerve function, calculated as a percentage of whisking amplitude compared to the control (unoperated) side. Notably, the rat whose held at low pressure (0-100mmHg) did not exhibit any facial nerve functional impairment, while the high-pressure rat showed immediate loss of facial nerve function with significant remaining impairment after 6 weeks of recovery. The medium pressure animal showed gradual reduction in facial nerve function to < 50% after applied compressive force on the nerve reached approximately 250mmHg, but saw a full recovery with decompression back to 100% 1 day after onset of palsy.**

Comparison of pressure readings from all three rats is shown Figure 16, demonstrating the need for intermittent fluid injection or withdrawal from the device to maintain pressures within the desired range. Pressure dropped to 0 mmHg for all rats on POD 8 because of surgical removal of device (i.e. removal of applied pressure on the nerve resulting in atmospheric pressure on the nerve). Additionally, the low-pressure animal began the study at 100mmHg, likely due to excess solute left in the device after sterilization. In spite of decompression with fluid withdrawal on POD1, pressure rose back to 100mmHg before dropping for unknown reasons, though notably staying within the 0-100mmHg range for the duration of the study.

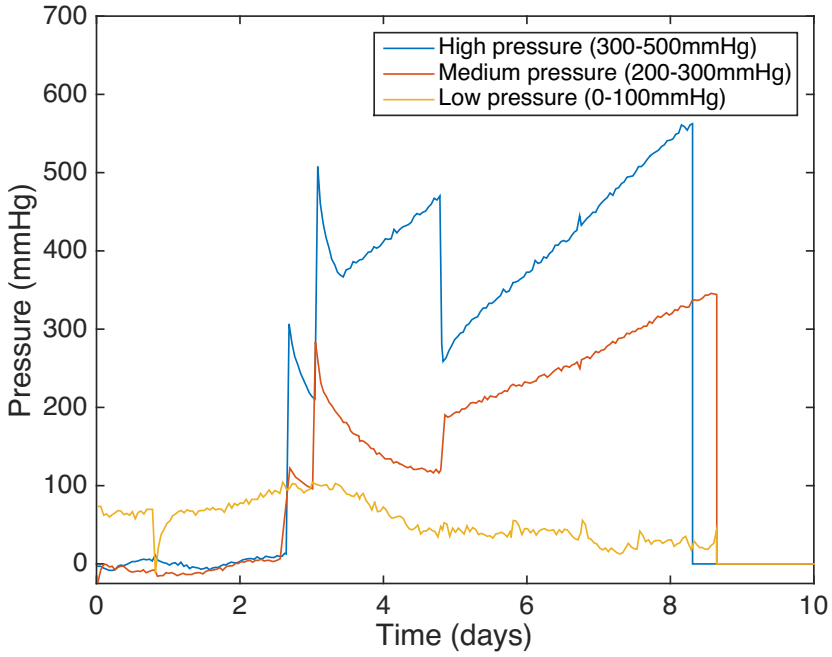

Figure 17: Pressures applied to the facial nerve read from each rat every hour, held at low (0-100mmHg), medium (200-200mmHg), and high (300-500mmHg) pressure ranges. Ability to adjust the pressure with fluid injection or removal is visible as rapid changes in reported pressure.

3.2.4 HISTOLOGY

Gross visualization of the nerves during device removal demonstrated full, thick, healthy nerve in the low-pressure animal (Figure 18a), appearing grossly identical to the nerve prior to implant (not shown). The nerve in the medium-pressure animal, however, was significantly thinned from before implantation (Figure 18b-c). The nerve in the high-pressure group was extremely thin (approximately half the thickness of the medium-pressure animal's nerve and approximately 10-20% the thickness of the low-pressure

animal's nerve), making it difficult to identify on gross inspection (not shown). The high-pressure animal's nerve was severed at the proximal end within the cuff; it was not clear during device removal whether the nerve had been severed in response to very light manipulation of the cuff during cuff removal, or spontaneously severed secondary to ischeamic degeneration from prolonged compression at high-pressure. At the time of this thesis submission, histology on nerve sections was still pending.

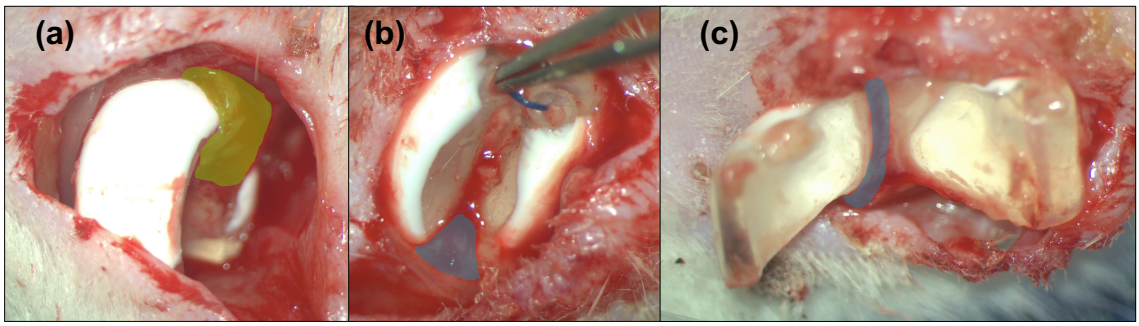

Figure 18: Images of gross dissection during cuff explant of low-pressure (nerve highlighted in green) and medium-pressure (nerve highlighted in blue) animals. (a) Closed cuff in low-pressure animal, showing thick, robust nerve. (b) Closed cuff in medium-pressure animal demonstrating pressurized cuff applying significant pressure circumferentially on the nerve (c) Opened cuff in medium-pressure animal, showing significantly thinner nerve after chronic compression at 200-300mmHg.

Histological evaluation of facial nerves 10 weeks after device explantation revealed varying amounts of injury and regeneration corresponding to amount of pressure applied (Figure 19). In the low-pressure nerve, axon caliber and count remained relatively unchanged from proximal to distal segments. The medium-pressure nerve showed evidence of partial axonotmesis and regeneration, as evidenced by the presence of numerous small-diameter regenerating axons in the distal segment. The high-pressure nerve showed evidence of near-complete third-degree Sunderland nerve fiber interruption with endoneurial tubule disruption and pervasive regenerating fiber presence.

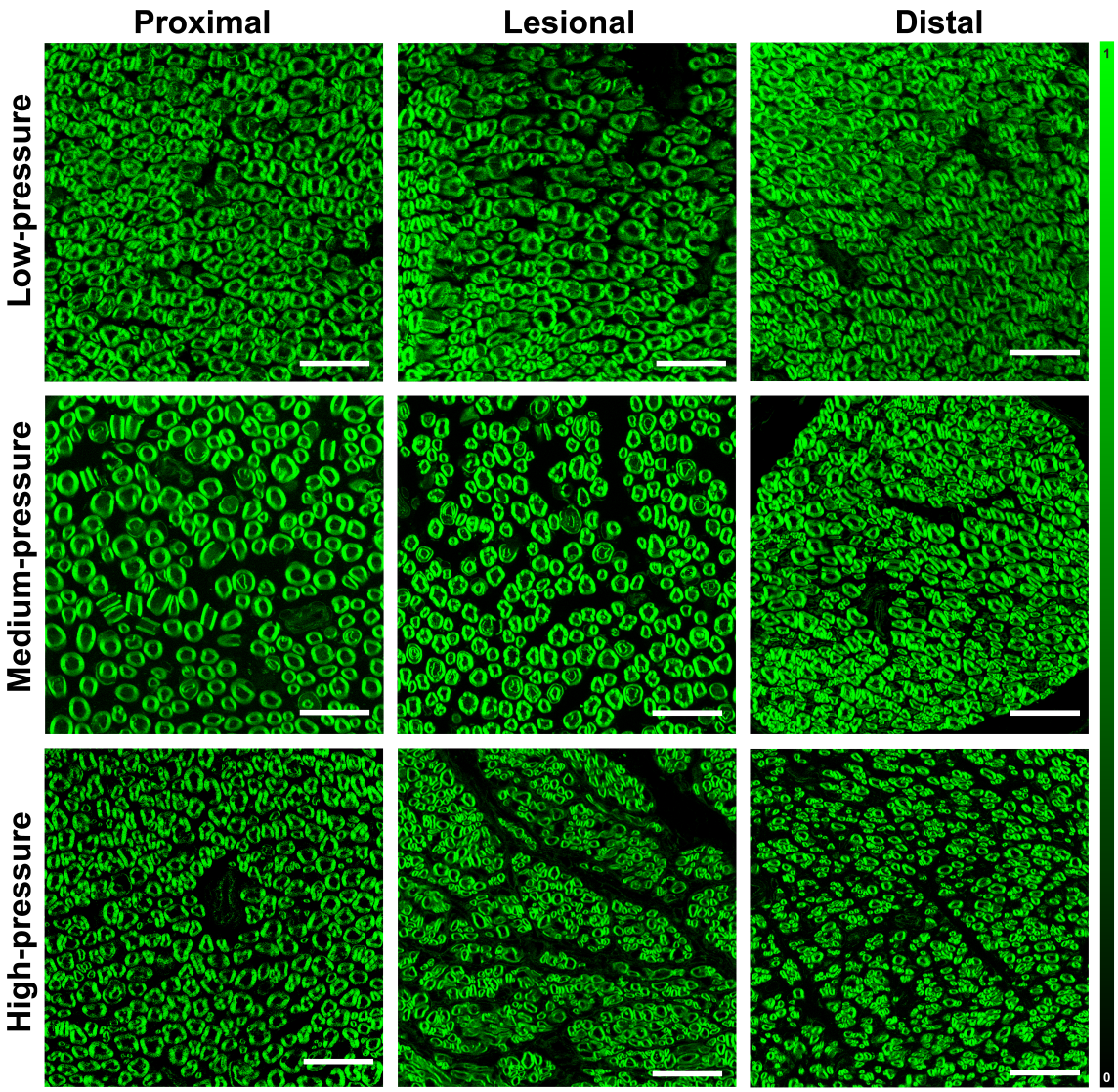

Figure 19: ***Confocal fluorescence imaging of rat facial nerves exposed to low, medium, and high-pressures from implanted pressure cuff.*** **Facial nerve axons exposed to low-pressures showed relatively unchanged axon caliber along the length of the nerve. Medium-pressure application revealed increased axon caliber variability with greater number of regenerating, small caliber axons. With high-pressure, near-complete axonal regeneration is suggested as the vast majority of stained axons are small, regenerating fibers. Scale bar: 30 µm, Color bar: normalized intensity value (0-1).**

4 DISCUSSION

4.1 *EX VIVO* AND *IN VIVO* VALIDATION

Ex vivo validation comparing the device to an external analog pressure monitor demonstrated the device has precise and accurate pressure readings to 20 mmHg or less, which is well within both the resolution attainable with the vascular cuffs and

physiologic variation in blood pressure between animals and over time within a single animal. Additionally, the devices showed this precision and accuracy with both chronically held pressure and rapidly changing pressure, demonstrating adequacy for modeling a dynamic system for induction of chronic compressive force. The device was shown to have adequate lifespan and datalogging capability required to run multiple experiments on different animals simultaneously spanning 6 or more weeks' duration, and could be adequately sterilized without damage.

The oncotic pressure-driven nature of the cuff, while somewhat limiting the precision with which the device may be pressurized, allows for the gradual development of compressive force on the nerve that more closely models the osmosis-driven neural edema secondary to inflammatory cell influx. Testing the device *ex vivo* in saline demonstrated the ability to reproducibly predict the final pressure attained in the system with the injection of a set amount of hypertonic glycerol solution, allowing for titration to desired pressure range for each device prior to implantation. The easily-accessible subcutaneous injection port also allows for additional fluid injection or withdrawal over the course of the study if correction is needed to maintain pressures within a desired range – while such fluctuations are not optimal, imperfect data acquisition is to be expected in any animal model and having a means to correct for undesired pressure changes is both practical and cost-effective. Additionally, while no data exists on the precise intratemporal pressures in Bell's palsy, some variation in any physiologic system is to be expected and does not invalidate subsequent results from the system if kept within a reasonable range.

Early studies demonstrated difficulty waterproofing the device and maintaining a seal between the 3D printed fitting and the printed circuit board. The addition of a press-fit for the 3D printed fitting and epoxy coating underneath the silicone coating of the entire device during manufacture resulted in devices that were shown to withstand implantation for multiple weeks with pressures of upwards of 500mmHg chronically without failure. Meeting these criteria was demonstrated to be more than adequate for the induction of functional loss in this model, demonstrating this device is robust and can yield reproducible results in multiple animal models without concern for high rates of device failure. However, in the event of device failure, the remote monitor described for precision pressurization can allow for sampling of pressures within the device.

The two *in vivo* studies described here demonstrated the sterilized devices can be implanted for at least 3 weeks without inducing seroma formation, tissue necrosis, or other signs of foreign body reaction other than a fibrotic capsule. Though this is sufficient for this model based upon human data suggesting efficacy of decompression surgery is lost after 14-21 days, it is likely that this device could be implanted for a much longer duration on the scale of months based upon device lifespan and toleration without exuberant foreign body reaction. Furthermore, data from all four animals showed no identifiable functional impairment postoperatively secondary to implantation. This suggests the nerve is robust enough and the device is tolerated well enough to isolate facial nerve functional loss through compression alone and further data will not be confounded by functional loss secondary to surgical implantation.

4.2 PRESSURE STUDIES

The first pressure study aimed at a "coarse search" for a pressure maximum and minimum demonstrated that (a) the nerve is able to tolerate some degree of compressive force over several days without overt functional impairment, and that (b) a high compressive force on the nerve induces rapid-onset functional loss with partial but incomplete functional recovery after decompression. This demonstrates the ability to recreate the clinical presentation of the approximately 15-30% of Bell's patients who experience incomplete functional recovery with this animal model. Additionally, animal held at medium pressure in the second "fine search" pressure threshold study demonstrated the model's ability to recreate the clinical presentation of the approximately 70-85% of Bell's patients who recover completely. The "fine search" study additionally found a pressure threshold of approximately 250-270 mmHg at which facial nerve function slowly dropped to 0% within approximately 72 hours, which very closely mirrors the progression of symptom onset in human Bell's palsy. Notably, this pressure was significantly higher than the average Lewis rat's systolic blood pressure (SBP) of 150 mmHg [62]. This is in line with the model, discussed earlier in the introduction, of a combination of early neurapraxia and progressive ischemic injury leading to poor electrical conductivity through the nerve that, if severe enough or left untreated, can lead to Wallerian degeneration and permanent functional loss. **Together, these data demonstrate this animal model is capable of modeling both the clinical presentation and long-term functional consequences of Bell's palsy in humans.**

4.3 LIMITATIONS

Though great care was taken to design the device to be robust and straightforward to use, it is still manufactured by manually combining a number of commercially available products, and is thus difficult to manufacture outside of an engineering or instrumentation facility. Ease of populating the printed circuit board is a surmountable obstacle, as all components can be sent to a commercial facility to place the microcontroller, sensor, and resistors/capacitors to place for a small additional cost, but the placement of the 3D printed fitting, cuff, port, and epoxy and silicone coatings are still performed manually and would likely not be cost-effective to automate. Additionally, during the completion of this thesis the microcontroller used (RFDuino Simblee) was discontinued and is no longer easily found commercially available. There are a number of other similarly sized microcontrollers with equivalent capabilities for sale, but would require a software and printed circuit board redesign.

Waterproofing the board, especially with creating a good seal between the 3D printed fitting and board, was a particularly difficult part of the design process because of the high shearing force from the fluid pressure inside it. While this was eventually solved with a combination of 3D printed fitting redesign and an epoxy layer on the board, it did interfere with early studies, including the first single-animal proof of concept study for minimum and maximum pressure range determination.

The variable permeability of the vascular occlusion cuff is also a significant limitation in rapid and precise usage of the device. While the gradual increase in pressure with oncotic-driven pressurization is likely more physiologically relevant, it makes titration of each individual device's pressure more difficult and error-prone, resulting in some extra variability in the three-animal pressure threshold determination study. This could potentially be averted with a more vascular cuff manufactured with increased crosslinking or of a different material, but currently the vascular cuffs used are the only cuffs of this small size available commercially.

Analyzing whisker movement adds an additional layer of variability to data processing, as well. Because rodents use their whiskers to explore their environment, having a particular interest in a segment of their environment will result in more whisking towards the area of interest, and thus can result in large variability between the whisker movements on each side of a healthy rat. For instance, if a rat's whisker is long enough

to touch part of the apparatus fixing them in place, they will whisk preferentially to that side to explore what that structure is. Additionally, while video tracking is a robust system to monitor whisker movement, there is some artifact introduced by tracking system inaccuracy. While such variability was minimized by trimming whiskers so they could not touch objects in the rat's local environment, bandpass filtering the data to only keep signals within known frequencies at which rats whisk, and smoothing this filtered data to minimize effect of rat movement or jitter from the whisker tracking algorithm, these factors still limit the precision with which nerve functional data could be analyzed.

While an animal model is excellent for studying neuropathy and neural regeneration in a controlled, randomized, and reproducible manner, it is limited in its translatability to human conditions. Rodents are known to undergo Wallerian degeneration approximately 2-4 times faster than humans, and additionally exhibit very robust neural regeneration[8, 9]. The distance across which nerve degeneration and regeneration occurs in this model is approximately 2 cm or less, significantly reduced compared to humans with Bell's palsy whose nerves course greater than 15 cm from their site of compression within the temporal bone to their most distal targets at the oral commissure.

It should be noted that, while presenting similarly, the pathogenesis of the presence or lack of permanent functional impairment is still poorly understood in humans, and thus similarities between human disease and this model cannot be verified to originate in the same mechanism (i.e. whether patients with permanent functional outcome have inherently higher intratemporal pressures or just experience neural compression for longer). Further testing needs to be done to determine whether chronic compression in this animal model at the minimum pressure threshold of approximately 250mmHg, rather than compression at suprathreshold pressures, could lead to incomplete recovery.

4.4 FUTURE WORK

In the future, we hope to apply this model to study the effect of timing of decompression surgery on long-term functional outcomes. Though the relationship between the timing of neural decompression and long-term functional outcomes in the rat may differ from that seen for humans, this work would establish whether a temporal relationship exists between decompression of the facial nerve (despite several days of compression at a pressure sufficient to induce a rapid-onset facial palsy) and long-term functional outcomes.

Finally, changing the pressures at which the devices are held during the study could be clinically relevant. For instance, patients who have more rapid symptom onset or have MRI findings indicative of increased neural pressures may benefit from more rapid decompression than patients who have slower onset of symptoms or more reassuring MRI findings, which may or may not be reflected in electrodiagnostic three days post-symptom onset. This model could result in the development of a three-dimensional dataset of pressure, time to decompression, and functional outcome, represented in Figure 20, that eventually could direct more nuanced guidelines for decompression surgery in humans.

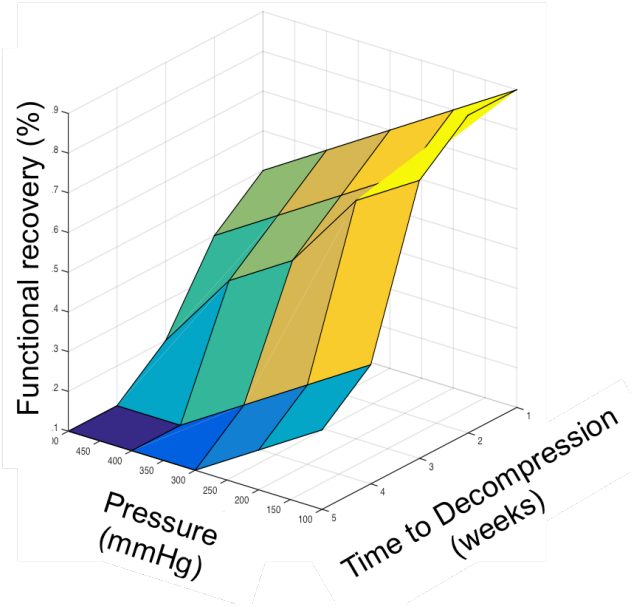

Figure 20: Idealized dataset graphically represented as a 3D plane showing the relationship between pressure applied to a nerve, duration of compression, and functional outcome.

5 CONCLUSION

Described is the design, manufacture, validation, and *in vivo* application of a miniaturized, wireless, implantable device that can be used to both induce and quantitatively monitor extrinsic pressure applied to a rodent peripheral nerve to model entrapment neuropathy. Functional loss induced in this model spanned a mild decrease in whisking amplitude to complete loss of whisking activity in a short time period, demonstrating the capacity of this model to induce a tunable range of motor neural dysfunction. Further, the model demonstrated the ability to reproduce a range of clinically-relevant long-term functional outcomes, ranging from complete return of normal

function, to partial return of function, to near-absent return of function. While we have used this device in a facial nerve model, this mechanism could be applied to any accessible nerve for longitudinal study, making it applicable for carpal tunnel, ulnar neuropathy, compartment syndrome or other entrapment neuropathies of the upper or lower extremities, or even cauda equina syndrome depending on the size of the animal model. Such a device provides the opportunity to investigate the mechanics behind compressive neuropathies in greater depth than has been previously possible, allowing improvements in understanding and treatment of such neuropathies.

In addition, this device is to the authors' knowledge the first demonstration of a fully implantable, wireless, open-source micro-controller and data transmitter used in the application of studying entrapment neuropathy. Due to its versatility in design and cost effective assembly, this device or similar designs may serve as research models for any implantable *in vivo* data relay or stimulator. With the occluding cuff placed around a vessel as opposed to a nerve, this device could be applied to the study of a variety of ischemic or vaso-occlusive disorders, including cerebrovascular accidents, hemodynamic shock, and free flap thrombosis. By virtue of the microprocessor's ability to transmit and receive data wirelessly and the board being custom-designed, the device can be easily redesigned and recoded, or the pressure sensor replaced with another physiologic monitoring system. Power consumption can be increased or decreased as needed with modifications of board components or sampling frequencies, allowing for the development of a wide variety of research and medical devices. The application of this device to future investigation, both of compression neuropathy and other *in vivo* stimulation or monitoring, could significantly improve our ability to gather quantitative, reproducible results from animal models of a wide variety of human diseases.

6 APPENDICES

6.1 ARDUINO CODE

6.1.1 IMPLANT

```
// Include relevant libraries for future needed commands
 #include "SimbleeCOM.h"
 #include <Wire.h>
 #include <SparkFun_MS5803_I2C.h>

 // Initialize values that will be needed throughout future commands
 MS5803 sensor(ADDRESS_HIGH);
 float temperature_c, temperature_f, pressure_abs, voltage;
 int cycles = 0;
 int delaytime = 1;

 // Requisite startup code for microprocessor to function
 void setup()
{
   // Define pins with which simblee will receive data input
   Wire.beginOnPins(22,28);

   // Initialize simblee microprocessor functionality
   SimbleeCOM.begin();

   // Start in low-power mode
   SimbleeCOM.mode = LOW_LATENCY;

   // Set simblee to transmit at lowest power level
   SimbleeCOM.txPowerLevel = -20;

   // Zero pressure sensor and initialize sensor for future
measurements
   sensor.reset();
   sensor.begin();
```

```
}
 // Main command of implant to read and transmit data, then sleep for
set amount of time
 void loop()
{

   // Zero pressure sensor
   sensor.reset();

   // Query sensor for pressure and temperature data
   temperature_f = sensor.getTemperature(FAHRENHEIT1, ADC_512);
   pressure_abs = sensor.getPressure(ADC_4096)*4;

   // Define external reference pin for voltage monitoring and read
voltage
   externalReference(AREF1);
   analogReference(EXTERNAL);
   voltage = analogRead(4)*2*3.65/1023;

   // Initialize string for data and battery voltage transmission
   String temp = "";

   //Add pressure, temperature, and battery voltage readings to string
   temp+=String(int(pressure_abs))+","+String(int(temperature_f))+","+S
tring(int(voltage*10));

   // Convert data string to character array
   // Note: this is performed because the microprocessor may only
transmit a character array, not a string
   char payload[temp.length()+1];
   temp.toCharArray(payload, temp.length()+1);

   // Send the character array with all data to any listening
datalogger(s)
   SimbleeCOM.send(payload, sizeof(payload));

   // Set implant to go into ultra-low power mode for a predefined
amount of time (here, 1 hour)
   delay(1);
```

```
    Simblee_ULPDelay(HOURS(delaytime));
    cycles = cycles + 1;

}
```

6.1.2 DATALOGGER

```
// Include relevant libraries for future needed commands
 #include "SimbleeCOM.h"
 #include <SPI.h>
 #include <SD.h>
 #include<stdlib.h>

 // Initialize values that will be needed throughout future commands
 const int chipSelect = 6;
 float P, T;

 // Requisite startup code for microprocessor to function
 void setup()
{
    // If connected directly to computer via USB, set up serial
    communication so future output is visible
    Serial.begin(9600);

    // Initialize simblee microprocessor functionality
    SimbleeCOM.begin();

    // If connected to computer via USB, communicate datalogger is
    online and finding SD card
    Serial.print("Initializing SD card...");

    // Default chip select pin is set to output
    pinMode(SS, OUTPUT);

    // Verify the SD card is present and can be written to, otherwise
    communicate failure
    if (!SD.begin(chipSelect))
{
      Serial.println("Card failed, or not present");
      return;
```

```
}
   Serial.println("card initialized.");
}

 // Placeholder loop, as at least one loop command is required for
 Simblee main function
 void loop() {
}

 // Command to store data and device serial number once it receives a
 data payload from an implant
 void SimbleeCOM_onReceive(unsigned int esn, const char *payload, int
 len, int rssi)

{
   // Saves implant serial number, as well as the payload and timestamp
   (seconds since start), to a string
   String dataStore = String(esn) + "," + String(payload) + "," +
   String(int(millis()/1000));

   // If connected to a computer, data is printed out for user to read
   in realtime
   Serial.println(dataStore);

   // Initialize a comma separated value file entitled datalog.csv for
   data input if not already present
   File dataFile = SD.open("datalog.csv", FILE_WRITE);

   // If the csv file is available, write data to it
   if (dataFile)
{
     dataFile.println(dataStore);
     dataFile.close();

}
}
```

6.2 ARDUINO LIBRARIES

These Arduino libraries are libraries used from outside commercial and noncommercial sources that are not standard libraries publicly available through Arduino (e.g. Wire.h, stdlib.h) or Simblee/RFDigital (e.g. SimbleeCOM).

6.2.1 SENSOR LIBRARY

```
/******************************************************************
MS5803_I2C.h
Library for MS5803 pressure sensors.
Casey Kuhns @ SparkFun Electronics
6/26/2014
https://github.com/sparkfun/MS5803-14BA_Breakout

The MS58XX MS57XX and MS56XX by Measurement Specialties is a low cost
I2C pressure sensor.  This sensor can be used in weather stations and
for altitude estimations. It can also be used underwater for water
depth measurements.

In this file are the function prototypes in the MS5803 class

Resources: This library uses the Arduino Wire.h to complete I2C
transactions.

Development environment specifics:
   IDE: Arduino 1.0.5
   Hardware Platform: Arduino Pro 3.3V/8MHz
   MS5803 Breakout Version: 1.0

**Updated for Arduino 1.6.4 5/2015**

Distributed as-is; no warranty is given.
******************************************************************/
#ifndef SparkFun_MS5803_I2C_h
#define SparkFun_MS5803_I2C_h

#include <Arduino.h>
```

```
// Define units for conversions.
enum temperature_units
{
   CELSIUS1,
   FAHRENHEIT1,
};

// Define measurement type.
enum measurement
{
   PRESSURE = 0x00,
   TEMPERATURE = 0x10
};

// Define constants for Conversion precision
enum precision
{
   ADC_256  = 0x00,
   ADC_512  = 0x02,
   ADC_1024 = 0x04,
   ADC_2048 = 0x06,
   ADC_4096 = 0x08
};

// Define address choices for the device (I2C mode)
enum ms5803_addr
{
   ADDRESS_HIGH = 0x76,
   ADDRESS_LOW  = 0x77
};

//Commands
#define CMD_RESET 0x1E // reset command
#define CMD_ADC_READ 0x00 // ADC read command
#define CMD_ADC_CONV 0x40 // ADC conversion command
#define CMD_PROM 0xA0 // Coefficient location

class MS5803
{
```

```
    public:
        MS5803(ms5803_addr address);
        void reset(void);  //Reset device
        uint8_t begin(void); //Collect coefficients from sensor

        // Return calculated temperature from sensor
        float getTemperature(temperature_units units, precision
        _precision);
        // Return calculated pressure from sensor
        float getPressure(precision _precision);
        uint16_t getCsensor(uint8_t i);
        uint16_t getCmicroP(uint8_t i);

    private:

        int32_t _temperature_actual;
        int32_t _pressure_actual;

        ms5803_addr _address;     // Variable used to store I2C device
        address.

        uint16_t coefficient[8];// Coefficients;

        void getMeasurements(precision _precision);

        void sendCommand(uint8_t command);  // General I2C send command
        function
        uint32_t getADCconversion(measurement _measurement, precision
        _precision);  // Retrieve ADC result

        void sensorWait(uint8_t time); // General delay function
};

#endif
```

6.3 MATLAB CODE: EXTRACTING DATA FROM DATALOG

```
%% Extract data

% Import the data from excel file
[~, ~, raw] = xlsread('/Users/Computer Name/Folder Path/DATALOG.xlsx');
raw(cellfun(@(x) ~isempty(x) && isnumeric(x) && isnan(x),raw)) = {''};

% Replace non-numeric cells with not-a-number (NaN) designation
R = cellfun(@(x) ~isnumeric(x) && ~islogical(x),raw);
raw(R) = {NaN};

% Create output variable (matrix with all raw data)
data = reshape([raw{:}],size(raw));

% Allocate imported array to column variable names
esn = data(:,1);
pressure = data(:,2);
temperature = data(:,3);
voltage = data(:,4);
time = data(:,5)./3600;

% Clear temporary variables
clearvars raw R;

% Initialize matrices and variables will need
listesn = []; % reference list of esns encountered (no. of devices
transmitting data)
dataarray = []; % array to store all data
% Note: design of dataarray is that each esn has all data stored in a
2D matrix, with each 2D matrix stacked to create a 3D matrix (see
accompanying figure for visualization)
reset = 0; % used to determine if particular esn's data has been stored

%% sort data into one matrix
% ROW = esn; COLUMN = data
% PAGES: 1 = P data; 2 = T data; 3 = voltage; 4 = time
```

```
% Iterate loop through all the esns logged
for i = 1:length(esn)
    reset = 0; % data has not been stored yet

    % At start of loop:
    if i == 1
        listesn(1) = esn(1); % record first esn in datalog as first in
        reference list of esns
        % store all data into data array
        dataarray(1,2,1) = pressure(1);
        dataarray(1,2,2) = temperature(1);
        dataarray(1,2,3) = voltage(1);
        dataarray(1,2,4) = time(1);
        dataarray(1,1,:) = esn(1); % reserve vertical slice for that
        device's future data
        reset = 1; % data has been stored, restart loop
    end

    % If find an esn that's already been put into data array matrix
    if reset == 0 % haven't already stored data
        for j = 1:length(listesn) % look through reference list of
        previously encountered esns
            if listesn(j) == esn(i) % found previously encountered esn
                % identify number of datapoints already stored for that
                esn (to avoid writing over data previously stored)
                totaldataperesn = nnz(dataarray(j,:,1));
                % store all data into data array
                dataarray(j,totaldataperesn+1,1) = pressure(i);
                dataarray(j,totaldataperesn+1,2) = temperature(i);
                dataarray(j,totaldataperesn+1,3) = voltage(i);
                dataarray(j,totaldataperesn+1,4) = time(i);
                reset = 1; % data has been stored, restart loop
            end
        end
    end
    % If have not encountered this esn before
    if reset == 0 % excludes other possibilities (data unstored, not
    first round, haven't seen ESN before)
        listesn = [listesn, esn(i)]; % add esn to reference list
```

```
        noesns = length(listesn); % updated no. of esns encountered
        % store data into data array
        dataarray(noesns,2,1) = pressure(i);
        dataarray(noesns,2,2) = temperature(i);
        dataarray(noesns,2,3) = voltage(i);
        dataarray(noesns,2,4) = time(i);
        dataarray(noesns,1,:) = esn(i); % reserve vertical slice for
        that device's future data
    end
end

%% display data
% all data plotted in separate figure, each device gets separate line
% Note: only displaying nonzero data because all other blank spaces in
data array are filled with placeholder zeros - this is to allow for
data array to contain different amounts of data from each device (e.g.
devices have different durations of implantation or different
transmission frequencies)

% Pressure vs time
figure(1)
for i = 1:length(dataarray(:,1,1))
   plot(nonzeros(dataarray(i,2:end,4)),nonzeros(dataarray(i,2:end,1)));
   hold on
end
xlabel('Time (hrs)');
ylabel('Pressure (mBar)');

% Temperature vs time
figure(2)
for i = 1:length(dataarray(:,1,1))
   plot(nonzeros(dataarray(i,2:end,4)),nonzeros(dataarray(i,2:end,2)));
   hold on
end
xlabel('Time (min)');
ylabel('Temperature (F)');

% Voltage vs time
figure(3)
```

```
for i = 1:length(dataarray(:,1,1))
   plot(nonzeros(dataarray(i,2:end,4)),nonzeros(dataarray(i,2:end,3)));
   hold on
end
xlabel('Time (min)');
ylabel('Battery Voltage (V)');
```

6.4 MATLAB CODE: COMPUTING NERVE FUNCTION FROM WHISKING DATA

For data analysis, the following code was automated in a loop to evaluate all csv files with whisking data from all 3 animals. Shown below is the content of the loop, rather than the entire sequence of loops, for simplicity.

```
% Extract whisking data from file and store right and left side data
file_location = ['/Users/Computer Name/Folder Path.csv'];
data = csvread(file_location,1,1);
RightSide = data(:,1);
LeftSide = data(:,2);

% define sampling frequency as 500 Hz
F=500;
% define new sampling rate of 100 Hz
Fs = F/5;

% FILTER RIGHT SIDED DATA
%Shift data to zero baseline
Whisker_R = RightSide(2:end)-RightSide(2);
%Resample raw data at 100Hz, also applying lowpass filter
%(8th order Chebyshev Type I, cutoff frequency (0.8*Fs/2)/F)
Whisker_RF = decimate(Whisker_R,5);
%Apply bandpass filter, keeping only data in whisking frequency (4-8Hz)
Whisker_RF = bandpass(Whisker_RF,[4,8],Fs);
%Smooth filtered data to minimize jitter from tracking program
Whisker_RF = smooth(Whisker_RF);

% REPEAT WITH LEFT SIDED DATA
Whisker_L = LeftSide(2:end)-LeftSide(2);
Whisker_LF = decimate(Whisker_L,5);
Whisker_LF = bandpass(Whisker_LF,[4,8],Fs);
Whisker_LF = smooth(Whisker_LF);

% Find maxima and minima of that particular day's whisking
max_R = max([max(Whisker_RF),abs(min(Whisker_RF))]);
max_L = max([max(Whisker_LF),abs(min(Whisker_LF))]);
```

```
% Finding all local maxima
[ypeaks_R,xpeaks_R] = findpeaks(Whisker_RF);
[ypeaks_L,xpeaks_L] = findpeaks(Whisker_LF);

% Finding all local Minima
[ytroughs_R,xtroughs_R] = findpeaks(-1.*Whisker_RF);
ytroughs_R = ytroughs_R.*-1;
[ytroughs_L,xtroughs_L] = findpeaks(-1.*Whisker_LF);
ytroughs_L = ytroughs_L.*-1;

% Aggregate all maxima and minima
ally_R = [ypeaks_R;ytroughs_R];
ally_L = [ypeaks_L;ytroughs_L];

% Find indices of maxima and minima that hit threshold for a whisk
ind_filtered_R = find(abs(ally_R)>threshold*max_R);
ind_filtered_L = find(abs(ally_L)>threshold*max_L);

% Aggregate all filtered maxima and minima meeting requirements
y_filtered_R = ally_R(ind_filtered_R);
y_filtered_L = ally_L(ind_filtered_L);

% Average of all maxima and minima (average whisker excursion)
Mean_R = mean(abs(y_filtered_R));
Mean_L = mean(abs(y_filtered_L));

% Calculating Power
[Pxx_R,F] = periodogram(Whisker_RF-mean(Whisker_RF),
[],512,Fs,'power');
[Pxx_L,F] = periodogram(Whisker_LF-mean(Whisker_LF),
[],512,Fs,'power');
Total_Power_Right = sum(Pxx_R);
Total_Power_Left = sum(Pxx_L);

% Calculate ratio of mean
RAmp = [RAmp,Mean_R];
LAmp = [LAmp, Mean_L];
RP = [RP,Total_Power_Right];
```

```
LP = [LP,Total_Power_Left];
```

The following figure graphically illustrates the process of filtering for whisking amplitudes, showing selection of all maxima and minima (top) and filtering those maxima and minima to identify all whisks with amplitude of 10% or more of the maximum whisk (bottom).

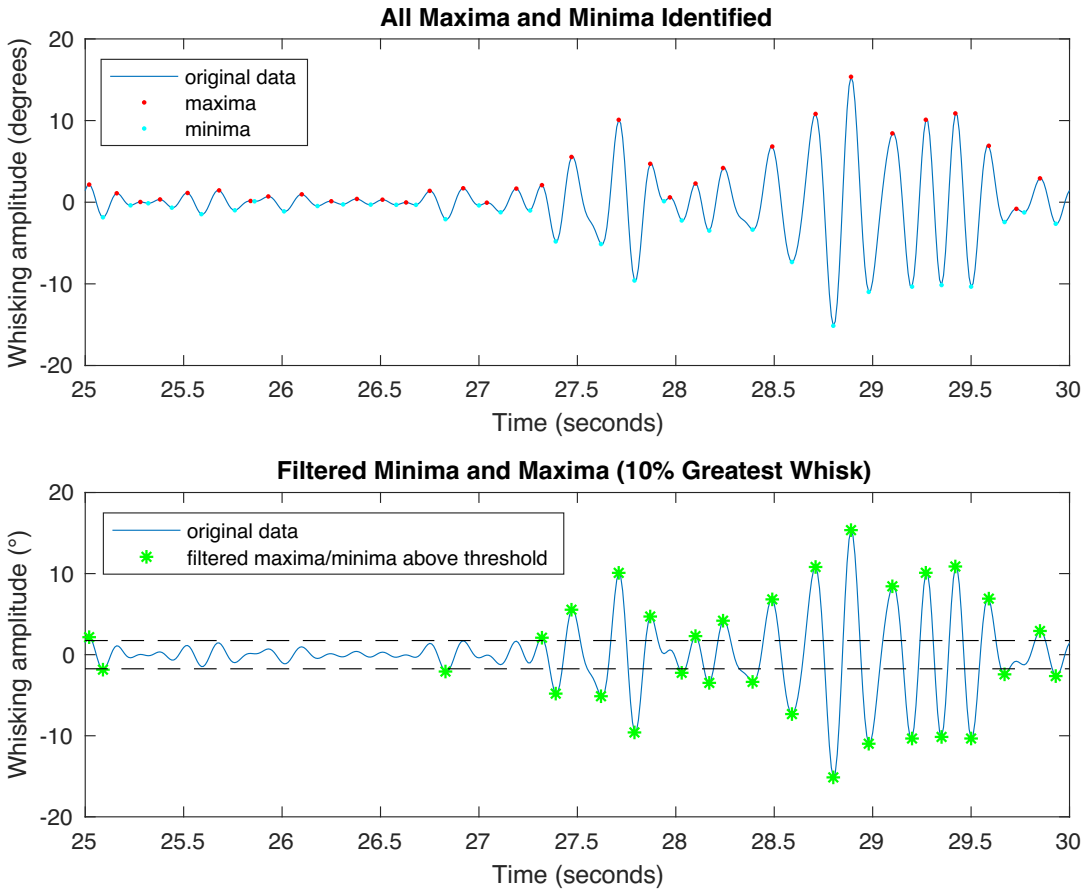

6.5 COMPONENT COST CALCULATIONS

6.5.1 COMPONENT COSTS OF IMPLANTABLE DEVICE

Component	Model # /Manufacturer	Per unit cost ($)
Printed Circuit Board	Custom design/Sunstone, Inc.	5.00
Wireless enabled microcontroller (Simblee)	RFD77101/RFDigital	20.00
Pressure sensor	MS5803-02BA/Servoflow	22.00
Magnetic Switch	KSK-1E66/MEDER electronic	11.00
Battery	CR1220/Energizer	2.00
Resistors/capacitors	Various manufacturers	2.00
3D-printed fitting	Custom design/FormLab 2	2.00
Epoxy coating	Two-Part Quick Set/Loctite, Inc.	1.00
Medical grade silicone coating	A-103/Factor II, Inc.	5.00
Vascular occluding cuff	OC-1.5/Access Technologies	100.00
Injection port	CP4-OC12/Access Technologies	50.00
	Per device total	**220.00**

6.5.2 COMPONENT COSTS OF WIRELESS RECEIVER

Component	Model # /Manufacturer	Per unit cost ($)
Microprocessor (Simblee)	RFD77201/RFDigital	30.00
microSD shield (Simblee)	RFD22130/RFDigital	16.00
USB shield (Simblee)	RFD22124/RFDigital	25.00
Battery shield (Simblee)	RFD22126/RFDigital	22.00
microSD card	SQUNC-064G/SanDisk	15.00
AAA batteries	Various manufacturers	2.00
	Per device total	**110.00**

6.6 PCB EAGLE SCHEMATIC AND BOARD LAYOUT

Simblee Microprocessor and External Pin Connectors

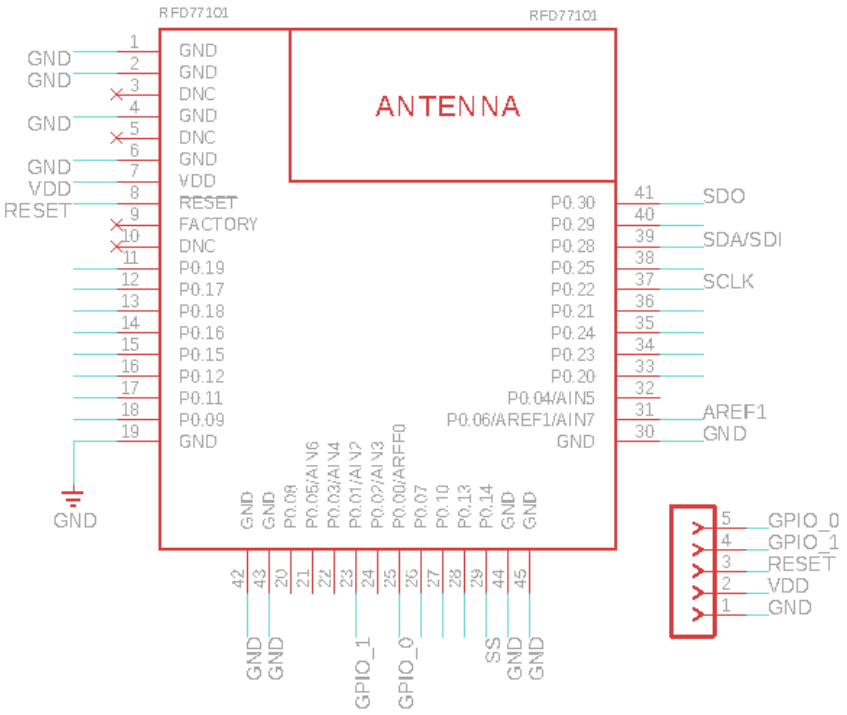

Pressure Sensor

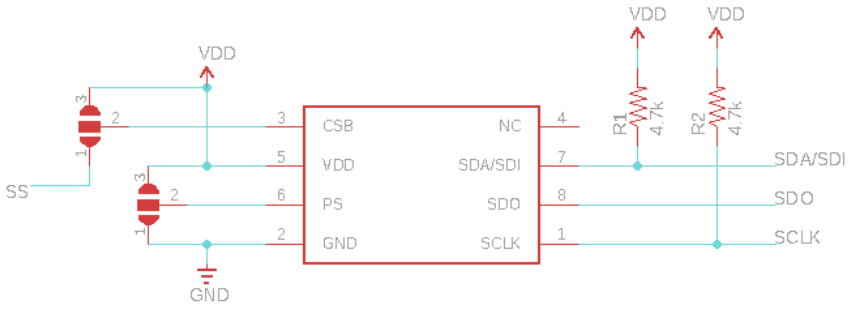

Magnetic Switch

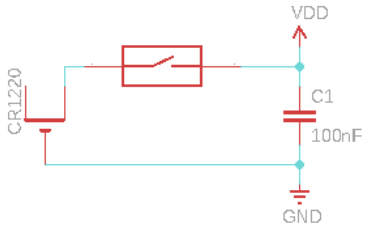

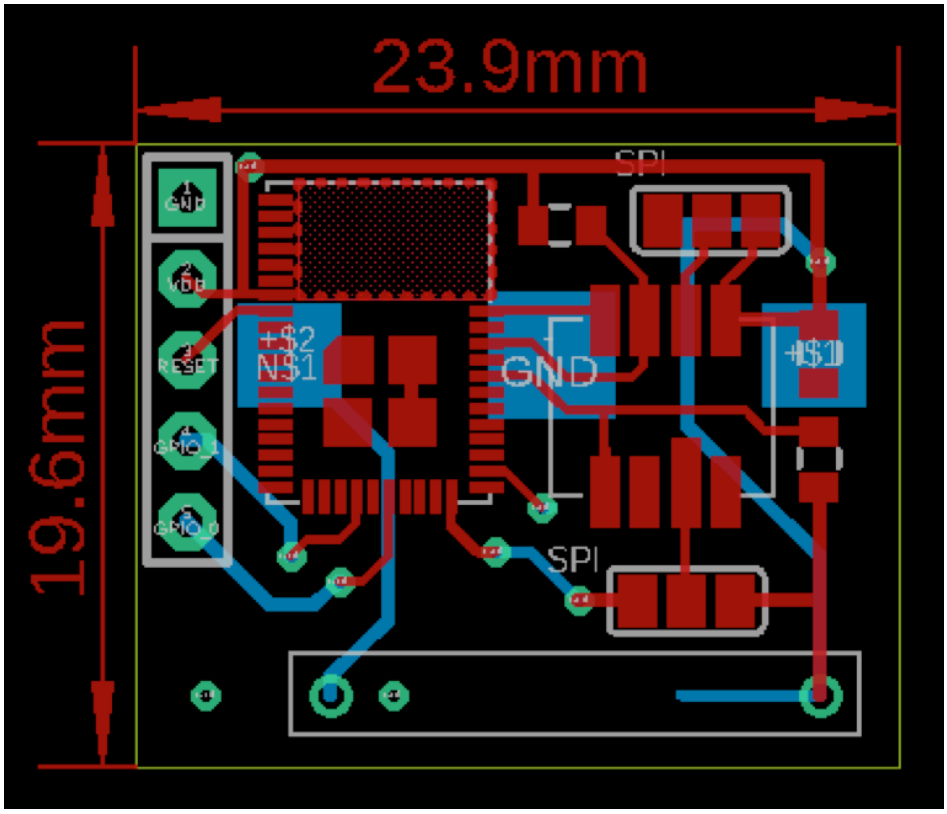
23.9mm
19.6mm
SPI
GND
VDD
RESET
GPIO 1
GPIO 0
+$2
N$1
GND
+$1
SPI

6.7 3D PRINTED PART SPECIFICATIONS

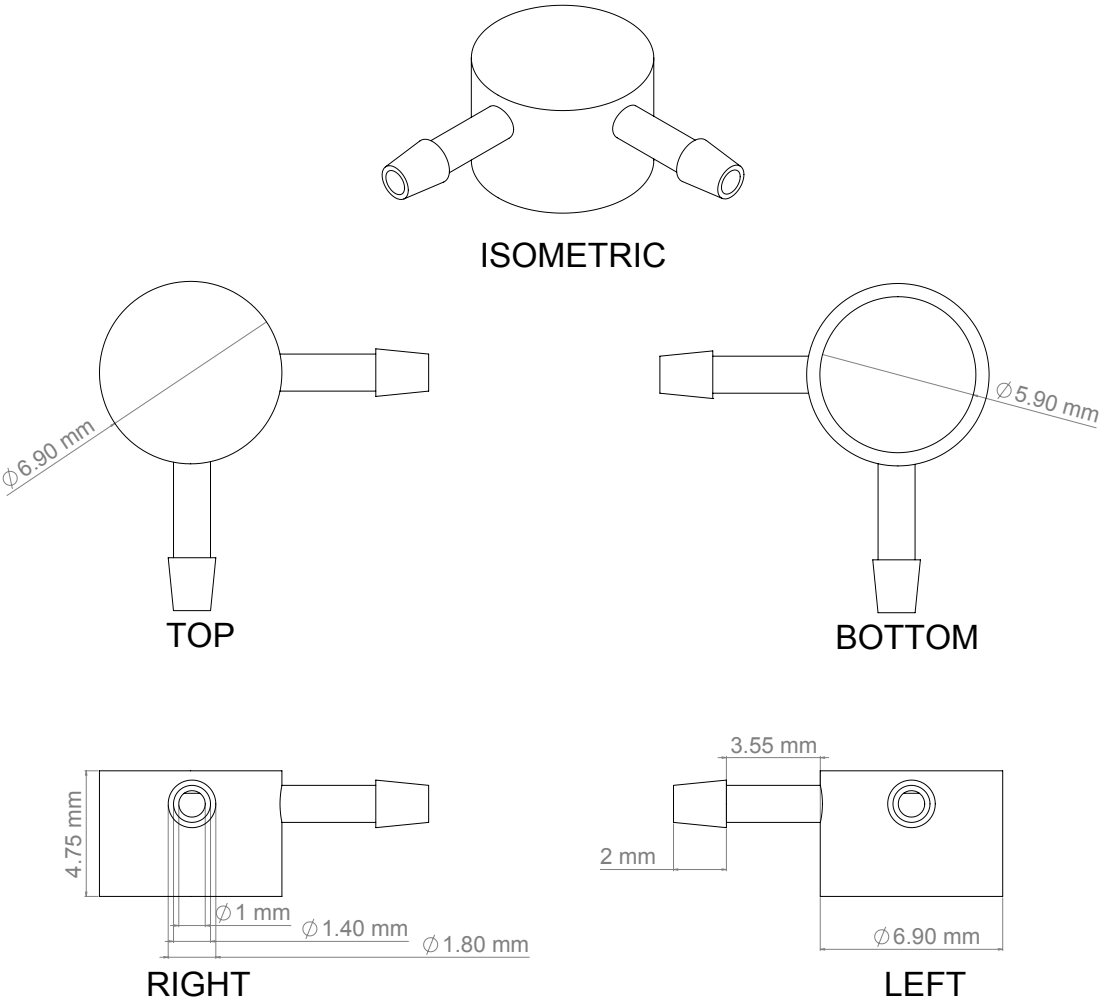

6.8 ACRYLIC JIG DESIGN SPECIFICATIONS

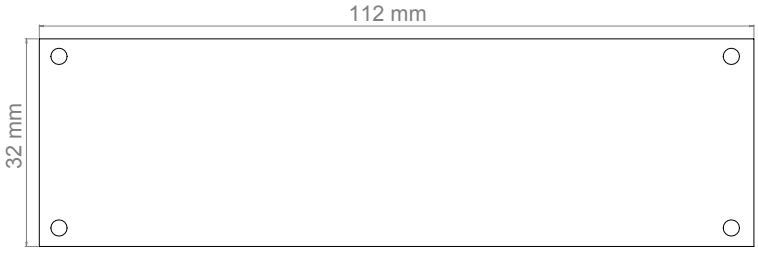

Base & Ceiling

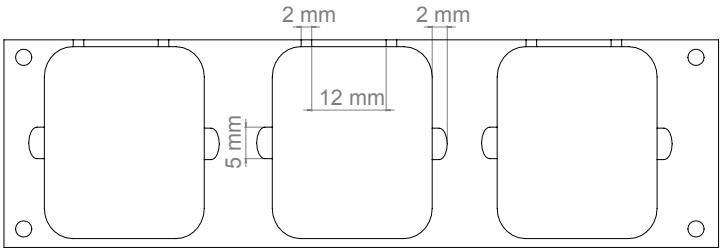

Wells with Tubing Ports & Phalanges

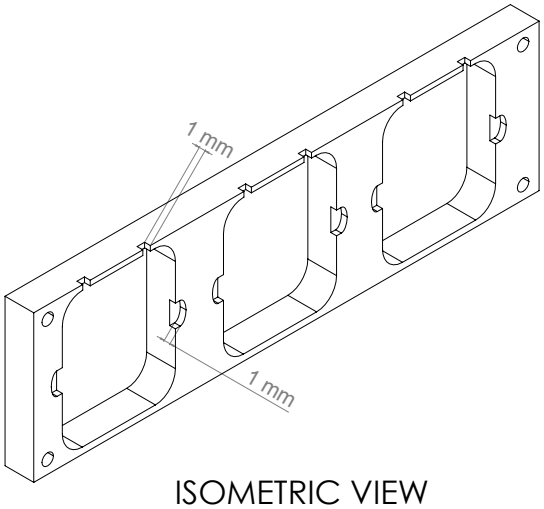

ISOMETRIC VIEW
Wells with Tubing Ports & Phalanges

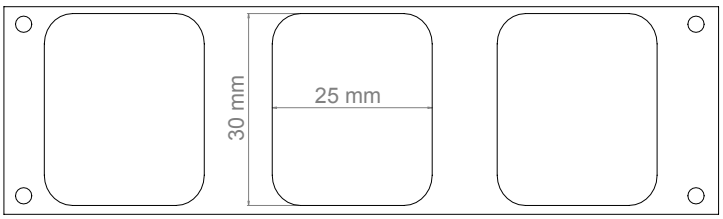

Wells Alone

6.9 EXTERNAL PRESSURE MONITORING

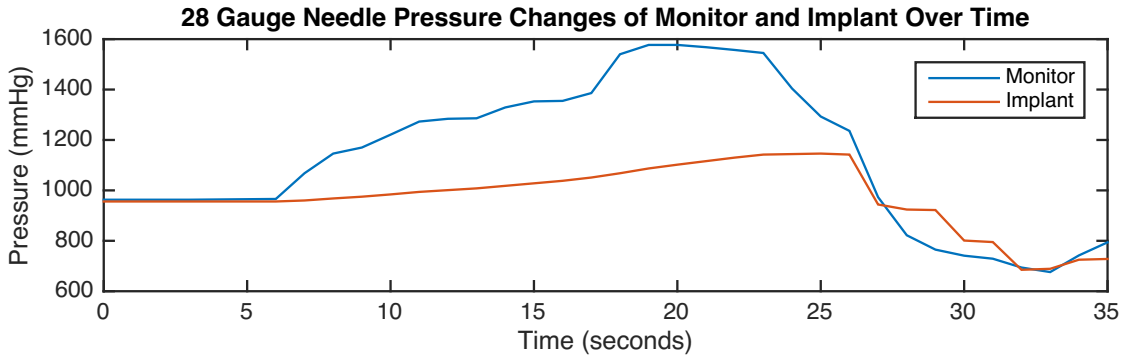

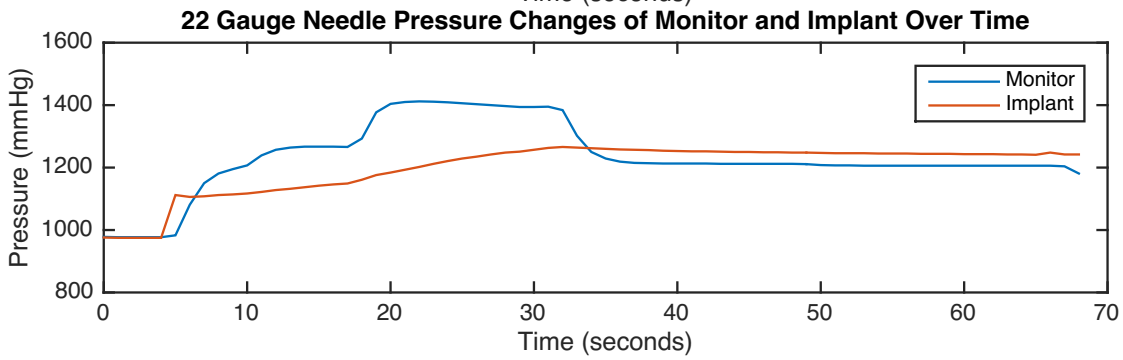

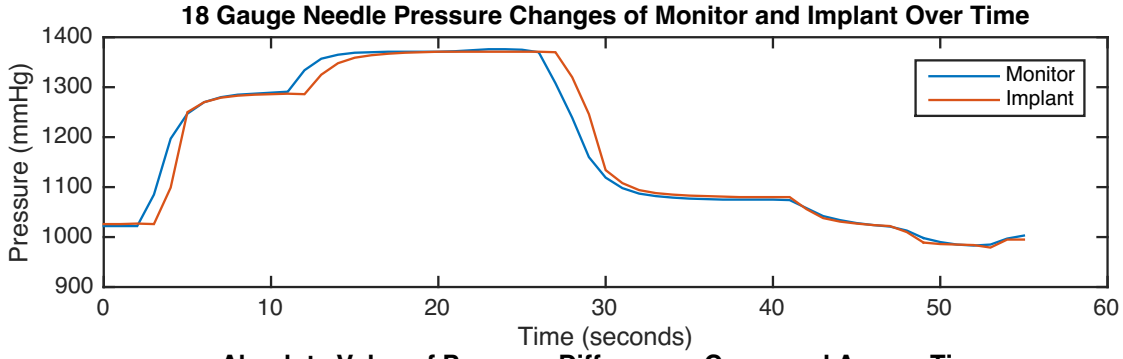

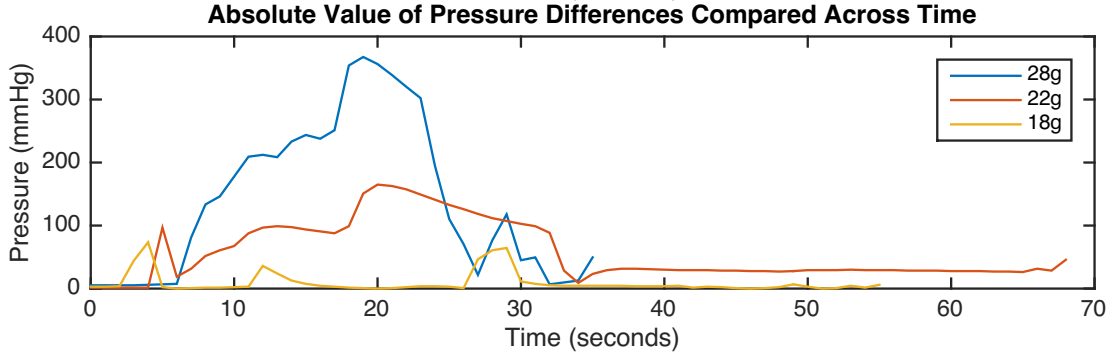

7 REFERENCES

1. Jowett, N. and T.A. Hadlock, *Contemporary management of Bell palsy.* Facial Plast Surg, 2015. **31**(2): p. 93-102.

2. Jowett, N. and T.A. Hadlock, *An Evidence-Based Approach to Facial Reanimation.* Facial Plast Surg Clin North Am, 2015. **23**(3): p. 313-34.

3. Jowett, N. and T.A. Hadlock, *A Contemporary Approach to Facial Reanimation.* JAMA Facial Plast Surg, 2015. **17**(4): p. 293-300.

4. Murakami, S., et al., *Bell's Palsy and Herpes Simplex Virus: Identification of viral DNA in endoneurial fluid and muscle.* Annals of Internal Medicine, 1997. **124**(1): p. 27-30.

5. Smouha, E., E. Toh, and B.M. Schaitkin, *Surgical treatment of Bell's palsy: current attitudes.* Laryngoscope, 2011. **121**(9): p. 1965-70.

6. Adour, K.K., *Decompression for Bell's palsy: why I don't do it.* European Archives of Oto-Rhino-Laryngology, 2002. **259**(1): p. 40-7.

7. Baugh, R.F., et al., *Clinical practice guideline: Bell's Palsy executive summary.* Otolaryngol Head Neck Surg, 2013. **149**(5): p. 656-63.

8. Coleman, M.P. and M.R. Freeman, *Wallerian degeneration, wld(s), and nmnat.* Annu Rev Neurosci, 2010. **33**: p. 245-67.

9. Gaudet, A.D., P.G. Popovich, and M.S. Ramer, *Wallerian degeneration: Gaining perspective on inflammatory events after peripheral injury.* Journal of Neuroinflammation, 2011. **8**(1): p. 1.

10. Seddon, H.J., *Three types of nerve injury.* Brain, 1943. **66**(4): p. 237-288.

11. Sunderland, S., *A classification of peripheral nerve injuries producing loss of function.* Brain, 1951. **74**(4): p. 491-516.

12. Lee, D.H., *Clinical Efficacy of Electroneurography in Acute Facial Paralysis.* J Audiol Otol, 2016. **20**(1): p. 8-12.

13. Gilden, D.H., *Clinical Practice: Bell's Palsy.* New England Journal of Medicine, 2004. **351**: p. 1323-1331.

14. Latinovic, R., Gulliford, M. C., & Hughes, R. A. C., *Incidence of common compressive neuropathies in primary care.* Journal of Neurology, Neurosurgery, and Psychiatry, 2006. **77**: p. 263-265.

15. Smith, B.E., *Focal and entrapment neuropathies*, in *Handbook of Clinical Neurology; Diabetes and the nervous system*. 2014.

16. Arnold, W.D.E., B. H, *Entrapment Neuropathies.* Neurologic Clinics, 2013. **31**(2): p. 405-424.

17. Peitersen, E., *Bell's Palsy: The Spontaneous Course of 2,500 Peripheral Facial Nerve Palsies of Different Etiologies.* Acta Oto-Laryngologica, 2002. **122**(7): p. 4-30.

18. Linder, T.E., W. Abdelkafy, and S. Cavero-Vanek, *The Management of Peripheral Facial Nerve Palsy: "Paresis" Vs. "Paralysis" and Sources of Ambiguity in Study Design.* Otology & Neurotology, 2010. **31**: p. 319-327.

19. Friedman, R.A., *The surgical management of Bell's palsy: a review.* American Journal of Otology, 2000. **21**(1): p. 139-44.

20. Nakatani, H., et al., *Initial lesions in Bell's palsy and Ramsay-Hunt syndrome.* Orl; Journal of Oto-Rhino-Laryngology & its Related Specialties, 2010. **71 Suppl 1**: p. 105-11.

21. Furuta, Y., et al., *High prevalence of varicella-zoster virus reactivation in herpes simplex virus-seronegative patients with acute peripheral facial palsy.* Clin Infect Dis, 2000. **30**(3): p. 529-33.

22. Pitkaranta, A., et al., *Detection of human herpesvirus 6 and varicella-zoster virus in tear fluid of patients with Bell's palsy by PCR.* J Clin Microbiol, 2000. **38**(7): p. 2753-5.

23. Stjernquist-Desatnik, A., E. Skoog, and E. Aurelius, *Detection of herpes simplex and varicella-zoster viruses in patients with Bell's palsy by the polymerase chain reaction technique.* Ann Otol Rhinol Laryngol, 2006. **115**(4): p. 306-11.

24. Mutsch, M., et al., *Use of the inactivated intranasal influenza vaccine and the risk of Bell's palsy in Switzerland.* N Engl J Med, 2004. **350**(9): p. 896-903.

25. Fisch, U., *Surgery for Bell's Palsy.* Arch Otolaryngol, 1981. **107**.

26. Gantz, B.J., et al., *Surgical Management of Bell's Palsy.* The Laryngoscope, 1999. **109**.

27. Yanagihara, N., et al., *Edematous swelling of the facial nerve in Bell's palsy.* Acta Oto-Laryngologica, 2000. **120**(5): p. 667-71.

28. Kang, T.S., et al., *Facial Nerve Grading Systems (1985-2002): Beyond the House-Brackmann Scale.* Otology & Neurotology, 2002. **23**(5): p. 767-771.

29. Vrabec, J.T., et al., *Facial Nerve Grading System 2.0.* Otolaryngol Head Neck Surg, 2009. **140**(4): p. 445-50.

30. Banks, C.A., et al., *Clinician-Graded Electronic Facial Paralysis Assessment: The eFACE.* Plast Reconstr Surg, 2015. **136**(2): p. 223e-230e.

31. Banks, C.A., et al., *Worldwide Testing of the eFACE Facial Nerve Clinician-Graded Scale.* Plast Reconstr Surg, 2017. **139**(2): p. 491e-498e.

32. Mannarelli, G., et al., *Electrophysiological measures in facial paresis and paralysis.* Operative Techniques in Otolaryngology-Head and Neck Surgery, 2012. **23**(4): p. 236-247.

33. Grogan, P.M. and G.S. Gronseth, *Practice parameter: Steroids, acyclovir, and surgery for Bell's palsy (an evidence-based review): report of the Quality Standards Subcommittee of the American Academy of Neurology.* Neurology, 2001. **56**(7): p. 830-6.

34. De Ru, J.A., P.A. Brennan, and E. Martens, *Antiviral agents convey added benefit over steroids alone in Bell's palsy; decompression should be considered in patients who are not recovering.* Journal of Laryngology & Otology, 2015. **129**(4): p. 300-6.

35. Shafshak, T.S., *The treatment of facial palsy from the point of view of physical and rehabilitation medicine.* Europa Medicophysica, 2006. **42**(1): p. 41-7.

36. Hohman, M.H. and T.A. Hadlock, *Etiology, diagnosis, and management of facial palsy: 2000 patients at a facial nerve center.* Laryngoscope, 2014. **124**(7): p. E283-93.

37. Hagino, K., et al., *Measurement of the facial nerve caliber in facial palsy: implications for facial nerve decompression.* Otology & Neurotology, 2011. **32**(4): p. 686-9.

38. Gantz, B.J., et al., *Intratemporal Facial Nerve Surgery*, in *Cummings Otolaryngology - Head and Neck Surgery, 6th edition*. 2015, Elsevier Saunders: Philadelphia, PA.

39. Fisch, U. and E. Esslen, *Total Intratemporal Exposure of the Facial Nerve; Pathological findings in Bell's palsy.* Arch Otolaryngol, 1972. **95**.

40. Liu, S., et al., *Study on relationship between operation timing and clinical prognosis of cases with Bell palsy.* Journal Of Clinical Otorhinolaryngology, Head, & Neck Surgery, 2013. **27**(13): p. 698-700.

41. Shapira, Y., L. Migirov, and J. Kronenberg, *Facial nerve decompression.* Harefuah, 2006. **145**(8): p. 557-60, 632.

42. Wu, S.H., et al., *Subtotal facial nerve decompression in preventing further recurrence and promoting facial nerve recovery of severe idiopathic recurrent facial palsy.* European Archives of Oto-Rhino-Laryngology, 2015. **272**(11): p. 3295-8.

43. Hato, N., et al., *Facial nerve decompression surgery using bFGF-impregnated biodegradable gelatin hydrogel in patients with Bell palsy.* Otolaryngology - Head & Neck Surgery, 2012. **146**(4): p. 641-6.

44. Cannon, R.B., et al., *Facial nerve outcomes after middle fossa decompression for Bell's palsy.* Otology & Neurotology, 2015. **36**(3): p. 513-8.

45. Bodenez, C., et al., *Facial nerve decompression for idiopathic Bell's palsy: report of 13 cases and literature review.* Journal of Laryngology & Otology, 2010. **124**(3): p. 272-8.

46. Li, Y., et al., *The effect of total facial nerve decompression in preventing further recurrence of idiopathic recurrent facial palsy.* European Archives of Oto-Rhino-Laryngology, 2015. **272**(5): p. 1087-90.

47. McAllister, K., et al., *Surgical interventions for the early management of Bell's palsy.* Cochrane Database of Systematic Reviews, 2013. **10**: p. CD007468.

48. Takahashi, H., et al., *Mouse Model of Bell's Palsy Induced by Reactivation of Herpes Simplex Virus Type 1.* Journal of Neuropathology and Experimental Neurology, 2001. **60**(6): p. 621-627.

49. Hazama, H., et al., *Compression of the facial nerve.* Archives of Otolaryngology, 1972. **95**(4): p. 346-349.

50. Rempel, D.M. and E. Diao, *Entrapment neuropathies: pathophysiology and pathogenesis.* J Electromyogr Kinesiol, 2004. **14**(1): p. 71-5.

51. Hadlock, T., et al., *A novel method of head fixation for the study of rodent facial function.* Exp Neurol, 2007. **205**(1): p. 279-82.

52. *Simblee Bluetooth Smart Module RFD77101 Datasheet.* 2017.

53. *MS5803-02BA Miniature Altimeter Module Specifications.* 2017.

54. Heaton, J.T., Kowaleski, J. M., Bermejo, R., Zeigler, H. P., Ahlgren, D. J., Hadlock, T. A. , *A System for Studying Facial Nerve Function in Rats through Simultaneous Bilateral Monitoring of Eyelid and Whisker Movements.* Journal of Neuroscience Methods, 2008. **171**(2): p. 197-206.

55. Guarin, D.L., Knox, C. J., Hadlock,, T. A., Jowett, N., *A novel approach for automatic whisker tracking in head-restrained rodents from high- speed videos*. 2018, Massachusetts Eye and Ear Institute.

56. Mohan, S., et al., *Fluorescent Reporter Mice for Nerve Guidance Conduit Assessment: A High-Throughput in vivo Model.* Laryngoscope, 2018. **128**(11): p. E386-E392.

57. Wang, W., et al., *A Rapid Protocol for Intraoperative Assessment of Peripheral Nerve Myelinated Axon Count and Its Application to Cross-Facial Nerve Grafting.* Plast Reconstr Surg, 2019. **143**(3): p. 771-778.

58. Schindelin, J., et al., *Fiji: an open-source platform for biological-image analysis.* Nat Methods, 2012. **9**(7): p. 676-82.

59. Stern, S.A.V., R. & Pratt, J.R., *Structure/Permeability Relationships of Silicon-Containing Polyimides*. 1989, National Aeronautics and Space Administration (NASA).

60. Zhang, H.C., A., *The Permeability Characteristics of Silicone Rubber*. 2006, Arlon Silicone Technologies Division: Bear, DE.

61. Volk, A., & Kähler, C.J., *Density model for aqueous glycerol solutions.* Experiments in Fluids, 2018. **59**(75).

62. Jessup, J.A., et al., *Attenuation of salt-induced cardiac remodeling and diastolic dysfunction by the GPER agonist G-1 in female mRen2.Lewis rats.* PLoS One, 2010. **5**(11): p. e15433.